Cell Reports

Resource

Pan-claudin family interactome analysis reveals shared and specific interactions

Graphical abstract

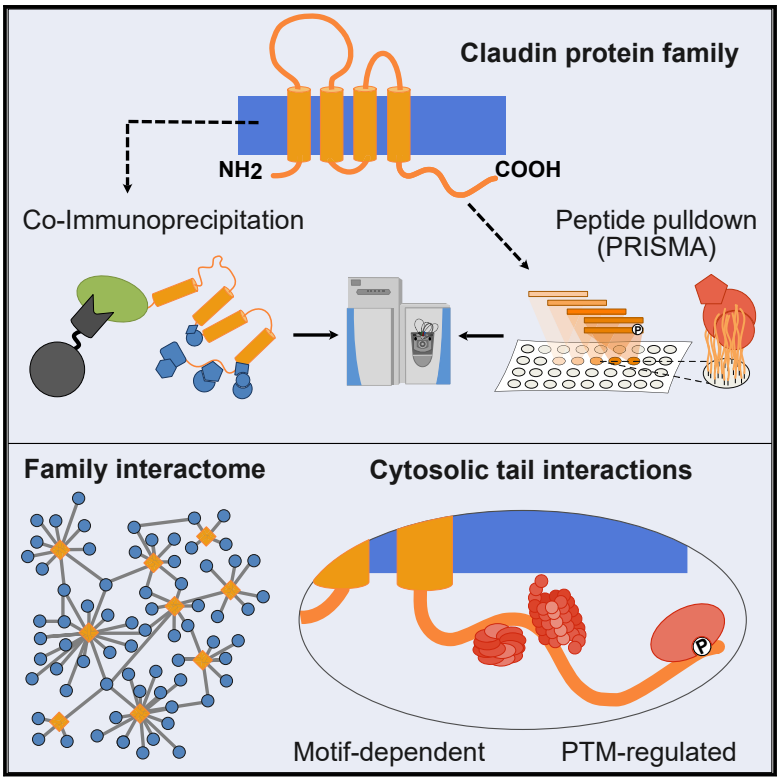

Highlights

- Comprehensive interactome of the entire claudin family
- PRISMA-based interaction mapping of the claudin C terminus
- The proteasome and the CCT complex interact directly with a subset of the claudins

Authors

Lorena Suarez-Artiles, Tilman Breiderhoff, Rossana Girardello, ..., Dominik Müller, Philipp Mertins, Gunnar Dittmar

Correspondence

dominik.mueller@charite.de (D.M.), philipp.mertins@mdc-berlin.de (P.M.), gunnar.dittmar@lih.lu (G.D.)

In brief

In a systematic analysis of the interactome of all members of the claudin family, which are central components of the tight junctions, Suarez-Artiles et al. show a direct interaction with the proteasome and the CCT complex and interactions between the claudin family members.

Suarez-Artiles et al., 2022, Cell Reports *41*, 111588
November 8, 2022
https://doi.org/10.1016/j.celrep.2022.111588

CellPress

Cell Reports

CellPress
OPEN ACCESS

Resource

Pan-claudin family interactome analysis reveals shared and specific interactions

Lorena Suarez-Artiles,[1] Tilman Breiderhoff,[2] Rossana Girardello,[3] Hannes Gonschior,[8] Sophie Rodius,[3] Antoine Lesur,[3] Ulf Reimer,[9] Evelyn Ramberger,[1,6,10,11] Daniel Perez-Hernandez,[3] Dominik Müller,[2,*] Philipp Mertins,[1,5,6,7,*] and Gunnar Dittmar[3,4,12,*]

[1]Max-Delbrück Center, Berlin, Germany
[2]Division of Gastroenterology, Nephrology and Metabolic Diseases, Department of Pediatrics, Charité-Universitätsmedizin Berlin, Berlin, Germany
[3]Proteomics of Cellular Signaling, Luxembourg Institute of Health, Strassen, Luxembourg
[4]Department of Life Sciences and Medicine, University of Luxembourg, Campus Belval, Luxembourg
[5]Berlin Institute of Health (BIH), Berlin, Germany
[6]German Cancer Consortium (DKTK), Partner Site Berlin, Germany
[7]German Centre for Cardiovascular Research (DZHK), Berlin, Germany
[8]Leibniz-Forschungsinstitut für Molekulare Pharmakologie (FMP), Berlin, Germany
[9]JPT GmbH, Berlin, Germany
[10]German Cancer Research Center (DKFZ), Heidelberg, Germany
[11]Department of Internal Medicine with Focus on Hematology, Oncology and Tumor Immunology,Charité-Universitätsmedizin Berlin, Berlin, Germany
[12]Lead contact
*Correspondence: dominik.mueller@charite.de (D.M.), philipp.mertins@mdc-berlin.de (P.M.), gunnar.dittmar@lih.lu (G.D.)
https://doi.org/10.1016/j.celrep.2022.111588

SUMMARY

Claudins are a family of transmembrane proteins expressed in epithelial tissues and are the major components of tight junctions (TJs), which define barrier properties in epithelia and maintain cell polarity. How claudins regulate the formation of TJs and which functions they exert outside of them is not entirely understood. Although the long and unstructured C-terminal tail is essential for regulation, it is unclear how it is involved in these functions beyond interacting with TJ-associated proteins such as TJ protein ZO-1 (TJP1). Here, we present an interactome study of the pan-claudin family in Madin-Darby canine kidney (MDCK)-C7 cells by combining two complementary mass spectrometry-based pull-down techniques creating an interaction landscape of the entire claudin family. The interaction partners of the claudins' C termini reveal their possible implications in localized biological processes in epithelial cells and their regulation by post-translational modifications (PTMs).

INTRODUCTION

Epithelial cells are attached laterally by a complex of intercellular junctions. Tight junctions (TJs) are the most apical cell-cell junctions, consisting of many integral membrane proteins and associated cytoplasmic proteins. They regulate the transepithelial paracellular transport of water and solutes and restrict the lateral diffusion of membrane proteins, maintaining the polarization in epithelial cells. Claudins are a family of tetraspan transmembrane proteins that represent the main structural components of TJs. In addition, they can localize to other regions of the basolateral plasma membrane and be part of focal adhesions. In cancer cells, there is solid evidence that claudin-1 to -4 can also be present in the nucleus (Cuevas et al., 2015; Dhawan et al., 2005; Ikari et al., 2014; Lee et al., 2010; Todd et al., 2015; Zwanziger et al., 2015). Claudins are involved in several pathologies of different natures. Mutations in claudin genes cause rare inherited disorders (such as familial hypomagnesemia with hypercalciuria and nephrocalcinosis [FHHNC], for claudin-16 and -19) (Konrad et al., 2006; Weber et al., 2000), and polymorphisms in claudin-1, -5, and -14 are associated with various polygenic diseases (De Benedetto et al., 2011; Sun et al., 2004; Thorleifsson et al., 2009). Aberrant expression, regulation, or localization of claudins is often observed in intestinal inflammatory diseases and is also related to metastatic progression in epithelial cancers (Kyuno et al., 2021; Oshima et al., 2008; Zeissig et al., 2007). In the case of infectious diseases, claudin-3 and -4 are receptors for the *Clostridium perfringens* enterotoxin (CPE) responsible for the symptoms of *C. perfringens*-associated gastrointestinal diseases, and, in the liver, claudin-1, -6, and -9 are co-receptors for hepatitis C virus entry in hepatocytes (Evans et al., 2007; Katahira et al., 1997; Morita et al., 1999; Zheng et al., 2007).

The claudin family has 27 genes in mammals and at least 23 in humans that encode proteins with a size range of 20–35 kDa, characterized by their four helical transmembrane domains. They contain two extracellular loops, the first one (ECL1) defining

the pore selectivity for the paracellular transport and the second (ECL2) important for interactions with claudins from adjacent cells; a short intracellular loop, and both N and C termini are intracellular. The N-terminal regions are very short, with few exceptions such as human claudin-16 (73 amino acids [aa]). The long, unstructured, intracellular C-terminal region varies between 25 and 111 aa, and its sequence is less conserved among the different claudins than other regions in the protein (Figure S1). It contains several post-translational modification (PTM) sites and a non-canonical PDZ domain-binding motif necessary for the interaction with the PDZ domain of TJs-associated proteins (Günzel and Yu, 2013). This binding motif differs from the class I (S/T-X-ΦCOOH) in that the affinity is defined by the C-terminal dipeptide (Y-V-COOH), present in most claudins, and by interactions with residues at positions −3, −4, and/or −6 (Zhang et al., 2006).

The cytosolic tail of claudins constitutes an intrinsically disordered region (IDR). IDRs have a flexible structure that allows a range of conformations facilitating interactions with different target molecules (Tompa et al., 2014). These regions can interact with multiple binding partners acting as hubs for proteins, and, in the case of transmembrane proteins, IDRs are also involved in the regulation of vesicle trafficking and the modulation of cell membranes (Cornish et al., 2020). Interactions in these regions are often mediated by short linear motifs (SLiMs), have low to moderate affinity but high specificity, and are frequently regulated by PTMs (Iakoucheva et al., 2004; Ivarsson and Jemth, 2019; Stein and Aloy, 2008).

The majority of claudin biology and physiology knowledge derives from mRNA expression studies, antibody-based detection, and functional studies in cell lines and animal models (Liu et al., 2016). These studies often focus on a particular isoform or a specific disease. However, the biological functions of claudins involve protein-protein interactions and regulation by PTMs, for which the approaches mentioned above fail to provide information. In contrast, mass spectrometry (MS)-based proteomics and, more specifically, affinity purification-MS (AP-MS) techniques allow the detection of functional protein interactions and have been used to map the interactome of several organisms (Hein et al., 2015; Keilhauer et al., 2015). Additionally, the recently developed Protein Interaction Screening on a Peptide Matrix (PRISMA) approach allows the study of protein interactions across unstructured regions similar to the cytosolic tail of claudins. PRISMA has previously been used to map binding partners along the sequence and PTM sites of CEBP transcription factors and to study the effect of disease-causing point mutations on protein interactions mediated by disordered regions (Dittmar et al., 2019; Hernandez and Dittmar, 2021; Meyer et al., 2018; Ramberger et al., 2021a, 2021b).

In this study, we combined two AP-MS methods, co-immunoprecipitation (coIP) and PRISMA, to investigate the interactions with the full-length and with the unstructured cytosolic tail of 25 human claudins, respectively. PRISMA was also used to study the influence of PTMs in the PDZ domain-binding motif of some claudins. Here, we present the first comprehensive interactome network of the entire claudin family, emphasizing the interactions with the cytosolic C-terminal regions. Our data provide insight into less-studied functions of claudins outside the TJ and the role of the long C termini of claudins beyond their interactions with the PDZ domain-containing TJ-associated proteins. Thus, our work expands the current knowledge in the field and serves as a resource for future studies related to claudins, their biology, and their implications in pathologies.

RESULTS

CoIP and PRISMA were combined for an extensive interactome study of the claudin protein family

The technical differences between coIP and PRISMA allow the study of different aspects of the interactome of claudins. CoIP experiments identify strong and stable interactions that resist the action of detergents and physical disruption of the cell. On the other hand, PRISMA provides information about less-stable interactions between proteins or protein complexes and linear motifs present in the unstructured cytosolic tail of claudins. Such SLiM-based interactions are frequently transient and regulated by PTMs (Figure 1A; Perkins et al., 2010). Gene Ontology (GO) enrichment analysis of combined interactome data of all claudin family members (see data below) highlights different subcellular locations of interactors detected by the two approaches. The top 15 most enriched GO Cellular Component (GOCC) categories show that coIPs primarily allow for the detection of proteins related to membrane-bound organelles, whereas PRISMA favors the identification of cytosolic proteins or interactors that are part of biomolecular complexes (Figure 1B). Combining the two orthogonal MS-based approaches yields complementary information about the claudin family interactome.

CoIP studies render a broad interaction map of the claudin family

Claudin coIPs were performed in Madin-Darby canine kidney (MDCK)-C7 cells heterologously expressing recombinant human claudin proteins N-terminally fused to YFP or CFP and cytosolic eGFP as a control. In total, 23 claudin coIPs were analyzed by MS and compared against the cytosolic control using a moderated t test to determine significant interactions for each member of the claudin protein family. In addition to the consensus significance cutoff of the adjusted p value <0.05, a more stringent second significance level was established for each pull-down corresponding to the adjusted p value that leaves only 5% of significant interactions for the eGFP control (Figures 2A and S2). Confocal microscopy confirmed cytosolic expression of the eGFP control as well as localization of recombinant claudins to the TJ in MDCK-C7 cells by co-localization with TJ protein ZO-1 (Figure S3). The coIP-based interactome contains 758 proteins significantly interacting with one or more claudins. The identified proteins were classified into 13 groups based on cellular compartment GO annotations extracted from the Database for Annotation, Visualization, and Integrated Discovery (DAVID) (Huang et al., 2009a, 2009b). This systematic classification system includes specific TJ and adherens junction (AJ)-related GO terms and broader terms such as localization to the plasma membrane and different organelles in the cell (Figure 2B; Table S1A). The first category, TJs, also covers interactions between different members of the claudin family. Claudins typically

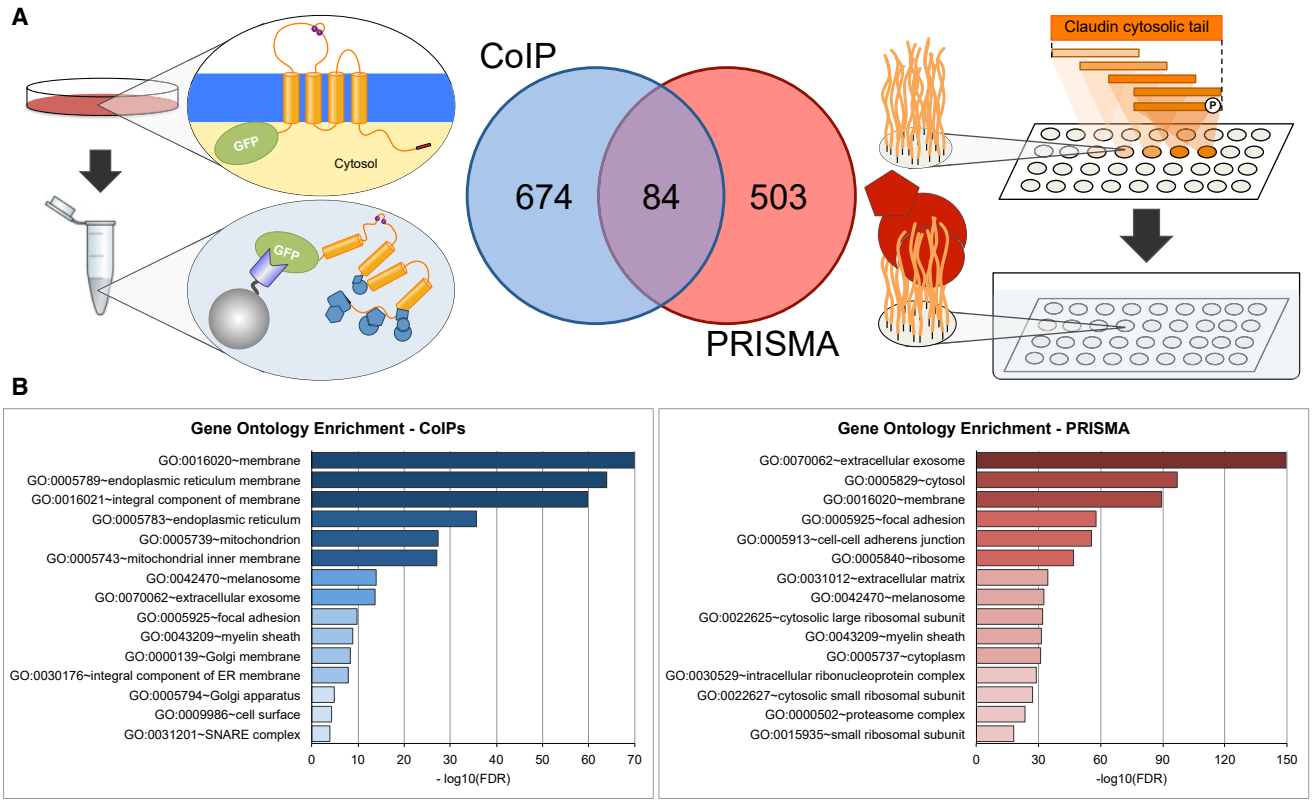

Figure 1. CoIPs and PRISMA provide complementary information about proteins from different cell compartments

(A) Conceptual differences between the coIP and PRISMA experiments. The overlap of the two different experimental setups is visualized in the Venn diagram. Significant PRISMA interactions before filtering by intensity binding profile.

(B) The GO enrichment analysis shows the complementary nature of the two approaches. While the coIPs of the full-length proteins from the cellular membrane show enrichment in membrane-bound interaction partners, the PRISMA-based approach shows the interaction of the claudin C termini with cytoplasmic proteins.

interact with each other within the same plasma membrane (*cis*) and with claudins present in the plasma membrane of adjacent cells (*trans*). These interactions can be respectively homomeric or homotypic between the same claudins but also heterotypic or heteromeric between different members of the claudin family. Our data confirm the previously described heterotypic interaction of claudin-3 with claudin-19B and -5 (Coyne et al., 2003; Daugherty et al., 2007; Milatz et al., 2017).

In addition, we identified novel heteromeric or heterotypic interactions between MDCK-C7 endogenous claudin-3 and overexpressed claudin-9 and claudin-18.2, and endogenous claudin-7 with overexpressed claudin-5 (Figure 2E). Besides claudins, the identified interactors annotated as TJ proteins serve as positive controls and, among others, include TJ protein ZO-1 (ZO-1 or TJP1), occludin (OCLN), MAGUK p55 subfamily member 7 (MPP7), InaD-like protein, and PALS1-associated TJ protein (PATJ). The TJ protein epithelial cell-adhesion molecule (EpCAM) interacts with claudin-7 in the gastrointestinal tract. However, co-localization of the two proteins was described as more prominent at the basolateral membranes (Ladwein et al., 2005). Several studies showed claudin-7 as part of macromolecular complexes forming focal adhesions along the basolateral membranes (Hagen, 2017), and intestinal cells of EpCAM-deficient mice and claudin-7 deficient mice show similar phenotypes with intestinal epithelial cells unable to attach to the underlying mucosa (Kozan et al., 2015). In this study, EpCAM was found interacting with claudins-8, -14, and -19B, suggesting that these claudins might be part of similar complexes outside TJs. Although it did not pass the initial, stringent significance cutoff, we identified the interaction of EpCAM with claudin-7 at a significance level of adjusted p value = 0.08. This might be a result of the overexpressed claudin-7 having to compete with the endogenous claudin-7 present in MDCK-C7 cells.

Claudins are also present in other regions of the plasma membrane and part of the focal adhesion complex. In the coIP dataset, 50 proteins are part of other cell-cell junctions besides TJs, and a total of 184 proteins are annotated as plasma membrane proteins. An interesting example is the glucose transporter GLUT-1 (SLC2A1), which was found to interact with most claudins except claudin-3, -11, -19A, and -24, and annotated as cell junction protein. This facilitative glucose transporter is in charge of the basal glucose intake, predominantly expressed in the blood-brain barrier (BBB), ensuring glucose transport into the brain (Klepper et al., 1999). In the kidney, basolateral GLUT-1 has been proposed to play a minor role in supporting

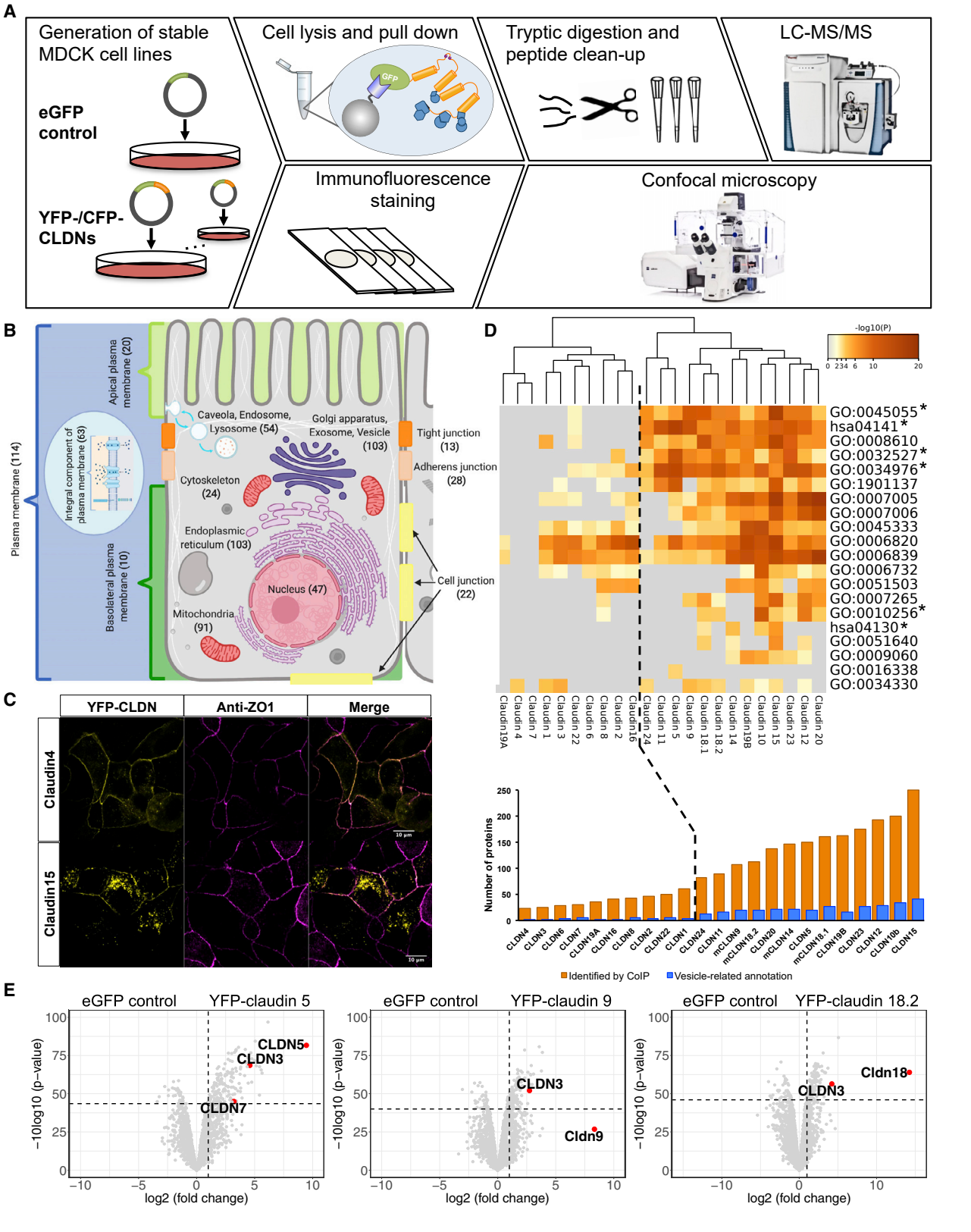

(legend on next page)

glucose reabsorption in the proximal tube of the nephron and, more importantly, take up glucose in further distal tubule segments for energy supply (Vallon, 2020). This finding is consistent with the strongest renal expression of GLUT-1 being found in the basolateral membrane of further distal tubule segments, with the highest levels detected in connective segments and collecting ducts in rat kidneys (Thorens et al., 1990). The interaction of GLUT-1 with the majority of claudins might be specific for the MDCK-C7 cell line that has a phenotype similar to the principal cells of the collecting duct. Still, these interactions point in the direction of a possible role of claudins in glucose homeostasis beyond the paracellular control of ion transport and outside the TJ.

As part of the TJ recycling and remodeling and claudin degradation process, claudins are also localized to intracellular vesicles. We identified 54 proteins related to internalization and lysosomal degradation as interactors of claudin proteins. Twelve of these proteins were also present in the apical junctional complex proximity quantitative proteomics dataset from Tan et al. (2020), including five small GTPases of the Rab family (RAB5B, RAB5C, RAB7A, RAB11FIP1, and RAB35) involved in different internalization pathways that lead to vesicle recycling or lysosomal degradation and can now be connected to specific claudins. Similarly, as tetraspan transmembrane proteins, claudins are synthesized and processed in the ER and Golgi and subsequently transported in vesicles to the plasma membrane. Thus, the 206 proteins annotated as related to these cellular compartments could be directly implicated in the biosynthesis pathway of claudins.

We unexpectedly found interacting partners of claudins from mitochondria and nucleus. It has been postulated that certain claudins, such as claudin-10b, can be found in the invaginations of the basal membrane of epithelial cells in the thick ascending limb (TAL) of the loop of Henle in kidneys, where a high number of mitochondria are required for energy-dependent transport (Milatz and Breiderhoff, 2017). We confirmed the interaction of the mitochondrial protein AFG3L2 with claudin-10 and MCU with claudin-23 using proximity ligation assay (PLA) assays (Figures 4B and S6). In the case of nuclear proteins, as previously mentioned, there is evidence of claudins localizing to the nucleus in cancer cells. Molecular studies also demonstrate a direct transcriptional role for nuclear claudin-1 in E-cadherin expression in cultured colon cancer cell lines (Dhawan et al., 2005). Additionally, an *in silico* analysis with cNLS mapper (Kosugi et al., 2009), a prediction tool for importin α-dependent nuclear localization signals (NLSs), showed that many mouse claudins contain putative NLS (Hagen, 2017). Among the 47 proteins identified annotated as nuclear, three are nuclear pore complex proteins (NUP88, NUP160, and NUP205) that might be involved in the recognition of the NLS and translocation of claudins to the nucleus.

Two distinct types of claudins behave differently in MDCK-C7 cells

The comparative analysis of the microscopy and the interactome data allows us to distinguish two types of claudins in terms of location and the number of different protein interactions. When overexpressed in MDCK-C7 cells, claudin-1 to -4, -6 to -8, -16, -19A, and -22 localize mostly at the TJ and plasma membrane and have a lower number of significant interactions (between 24 for claudin-4 and 61 for claudin-1). On the other hand, claudin-5, -9, -10, -11, -12, -14, -15, -18.1, -18.2, -19B, -20, -23, and -24 have a higher number of significant interactions (82 for claudin-24 and 250 for claudin −15) and a wider localization in the cell, not only at the TJ and plasma membrane but also intracellularly (Figures 2C and S3). A Metascape enrichment analysis (Zhou et al., 2019) identified two clusters of claudins based on GO terms related to exocytosis and ER. These clusters also separate claudins into two groups corresponding to a lower and higher number of significant interactions. The same two groups of claudins are maintained when looking only at proteins with GOCC annotations related to vesicles (Figure 2D). However, it is not clear whether this accumulation in cytosolic vesicles responds to a higher expression, a competition with the endogenous claudins for incorporation into the TJ, or a faster turnover of these claudins in particular.

Proteasome and CCT/TRiC protein complexes interact with the cytosolic C-terminal tail of claudins

Proteins interacting with the disordered C-terminal tail of the different claudins were identified using the PRISMA methodology (Dittmar et al., 2019; Ramberger et al., 2021a, 2021b). Briefly, the aa sequence of the claudins' C termini (Figure 3A)

Figure 2. CoIP experiments provide a comprehensive interaction map of the claudin family

(A) Workflow for coIP experiments. Stable MDCK-C7 cell lines overexpressing recombinant claudins (N-terminal YFP/CFP fused) or cytosolic eGFP as a control were used to study the interactome of each member of the claudin family by pull-downs with GFP-Trap nanobodies and liquid chromatography-tandem mass spectrometry (LC-MS/MS). In parallel, localization of the recombinant claudins in the cell was monitored by confocal microscopy.

(B) Hierarchical classification of the identified significant interactors into 13 different groups by their Gene Ontology Cellular Component (GOCC) annotations. The number of proteins per group is listed in brackets. Created with BioRender.com.

(C) Confocal microscopy images show claudin-4 localization mainly at the cell membrane, in contrast to claudin-15, which has an additional strong signal in the cytosol.

(D) Metascape enrichment analysis of coIP results reveals two main clusters of claudins. Below: the two clusters differentiate in the total number and vesicle-related interactors. Asterisks (*) indicate terms and pathways related to vesicular transport and ER. GO:0045055, regulated exocytosis; hsa04141, protein processing in ER; GO:0008610, lipid biosynthetic process; GO:0032527, protein exit from ER; GO:0034976, response to ER stress; GO:1901137, carbohydrate derivative biosynthetic process; GO:0007005, mitochondrion organization; GO:0007006, mitochondrial membrane organization; GO:0045333, cellular respiration; GO:0006820, anion transport; GO:0006839, mitochondrial transport; GO:0006732; coenzyme metabolic process, GO:0051503, adenine nucleotide transport; GO:0007265, Ras protein signal transduction; GO:0010256, endomembrane system organization; hsa04130, SNARE interactions in vesicular transport; GO:0051640, organelle localization; GO:0009060, aerobic respiration; GO:0016338, calcium-independent cell-cell adhesion via plasma membrane cell-adhesion molecules; GO:0034330, cell junction organization.

(E) Heteromeric/heterotypic interactions between overexpressed and MDCK-C7 endogenous claudins using three replicates.

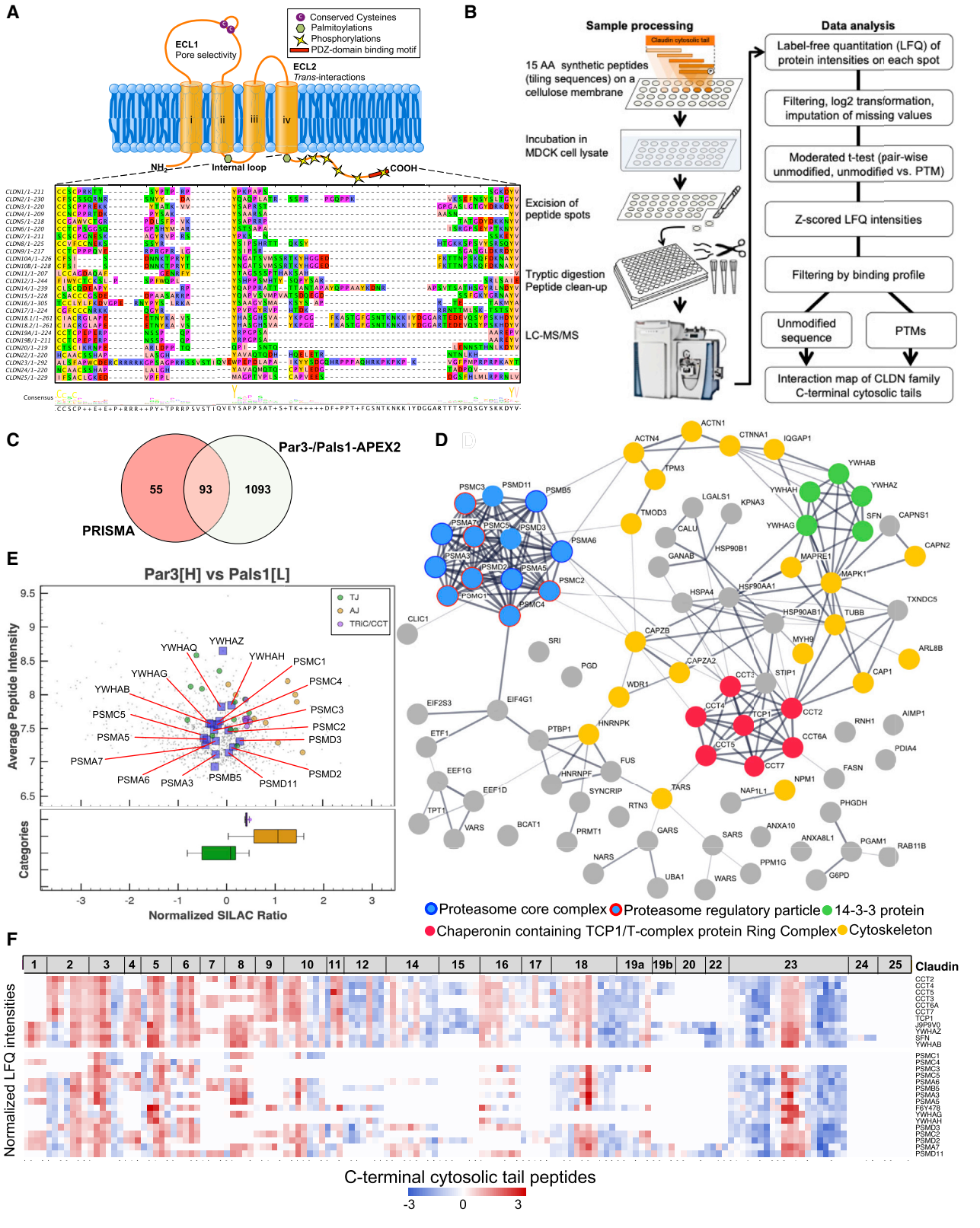

(legend on next page)

was used to generate a library of 15-aa-long overlapping peptides with a 5-aa window shift mapping the cytosolic tails of the different members of the claudin family. Then 169 peptides (unmodified and modified) were synthesized by spot-synthesis (Frank, 1992) on a cellulose membrane that was incubated with MDCK-C7 nuclei-depleted cell lysate. Interacting proteins were identified by MS, and the data were integrated to create a general interaction map (Figure 3B). Unmodified peptides were used to study interactions with linear motifs present in claudin C-terminal IDRs. The significant interactions identified were filtered according to intensity profiles that fit a SLiM-dependent type of interaction (Figure S4). This means interaction across three to four overlapping peptides with the highest intensity in the middle. In total, PRISMA identified 148 SLiM-dependent interactors of claudin cytosolic tails (Figure S5; Table S1B).

A comparison of the claudin PRISMA dataset with an APEX2-based proximity interactome of TJ proteins Pals1 and Par3 (Tan et al., 2020) revealed an overlap of 93 proteins (Figure 3C). Among those proteins were 13 members of the proteasome complex, five subunits of the catalytic core particle (PSMA6, PSMA7, PSMA5, PSMA3, and PSMB5), and eight subunits of the regulatory particle (PSMC2, PSMC1, PSMC4, PSMC3, PSMC5, PSMD2, PSMD3, and PSMD11), seven members of the chaperonin-containing TCP1 (CCT/TriC) complex (TCP1, CCT2, CCT3, CCT4, CCT5, CCT6A, and CCT7), and five out of the seven members of the 14-3-3 family (SFN, YWHAB, YWHAG, YWHAH, and YWHAZ) (Figure 3D). Tan et al., (2020) also showed that these three groups of proteins seem to localize at the intersection of TJ and AJ (Figure 3E). Interestingly, the protein complexes found are differentially interacting with the cytosolic tail of a subset of the claudins but not with the others (Figure 3F). The interactions of the claudins with the proteasome and CCT/TriC complexes are summarized in Table 1.

PLAs confirm the interaction of CCT/TRIC and proteasome subunits with claudin-3

Next, we validated the MS-based interactome data with *in situ* PLA. PLA in MDCK-C7 stable cell lines confirmed the differential interaction of the CCT/TriC chaperonin complex subunits CCT2 (TCP-1-beta) and CCT6 (TCP-1-zeta) with claudin-3 but not claudin-1 or -12 as identified by the PRISMA screen. Similarly, the interaction of the proteasome complex subunit PSMA3 with claudin-3 but not claudin-1 was confirmed. In both cases, the quantification of PLA counts per cell showed enhanced binding in claudin-3 compared with claudin-1 and claudin-12 (Figures 4A and 4C).

The ubiquitin/proteasome system (UPS) has been shown to regulate the fate of various membrane proteins, including AJ and TJ transmembrane proteins, by mono- or polyubiquitination leading to endocytosis and recycling/degradation via the lysosome or degradation by the proteasome (Cai et al., 2018). Although the ubiquitination and subsequent endocytosis and lysosomal degradation of some members of the claudin family have been characterized, so far, only claudin-5 is known to be degraded both in an Ubiquitin-proteasome-dependent manner and by the Ubiquitin-independent lysosomal pathway (Mandel et al., 2012; Traweger et al., 2002). On the other hand, cytosolic proteins that are part of the cell-cell junctions are mostly polyubiquitinated and degraded via the proteasome (Cai et al., 2018; Chen et al., 2014). Thus, the identification of the proteasome complex interacting with unmodified peptides from the C-terminal region of claudins indicates that the role of these interactions could be the degradation not of the claudin itself but of cytosolic ubiquitinated proteins in the vicinity. In addition, there is evidence showing the role of the UPS and local protein degradation in synaptic plasticity (Hegde, 2004). Similarly, TJs are dynamic structures with constant trafficking and recycling of proteins between the cytoplasm and the cell surface. The interaction of the subunits of the proteasome core complex with some of the claudins might point to proteasome recruitment to the TJs. Localization of the proteasome at the TJs would allow for faster degradation events without the dependency on diffusion to reach the proteasome for degradation. Localized degradation has previously been shown in neurons as part of synaptic degradation. Therefore, we speculate that the association of the proteasome with the TJs might point to localized degradation foci, at least in epithelial cells.

We found the CCT/TRiC complex to interact with several claudins. However, the role that this complex has in the biology of claudins and TJs remains unknown. The CCT/TriC chaperonin complex folds approximately 10% of all cytosolic proteins, and WD-repeat proteins have been described as important CCT/TriC substrates (Li and Roberts, 2001). WD-repeat proteins are involved in a wide range of cellular functions, such as signal transduction, cytoskeletal assembly, and regulation of vesicular trafficking, among many others. One of the cytoskeletal proteins found as interacting with claudins in the PRISMA dataset is the WD-repeat-containing protein 1 (WDR1 or actin-interacting

Figure 3. PRISMA reveals protein complexes interacting with the cytosolic tail of some claudins

(A) The cytosolic C termini of claudins varies in length and sequence across the different members of the protein family. Full alignment in Figure S1.

(B) PRISMA workflow used to map interactions of the cytosolic tail of claudins and to study the influence of phosphorylations. After normalization of the LFQ intensity values, proteins with adjusted p value <0.05 were filtered based on (1) intensity binding profile, defined by interaction across three to four unmodified overlapping peptides with the highest intensity in the middle; (2) changes in the intensity of proteins identified in unmodified and phosphorylated peptide pull-downs.

(C) Overlap between proteins found interacting with unmodified claudin peptides (PRISMA) and a previous dataset of proteins related to the apical junction complex identified by quantitative proximity proteomics (QPP) (Tan et al., 2020).

(D) String network of the proteins overlapping interactions of the datasets compared in (C).

(E) Distribution of proteasome and CCT/TRiC complex subunits, and 14-3-3 proteins within the apical junction complex determined by QPP. Average log10 peptide intensities over the average log2(H/L) normalized SILAC ratios for all proteins identified by Tan et al., (2020). Median distribution of proteins from the categories adherens junction (AJ) and tight junction (TJ). From the interactive online portal Par3-Pals1 HCP (Tan et al., 2020).

(F) Intensity map of the proteins mentioned above identified by PRISMA. Uniprot entries J9P9V0 and F6Y478 correspond to 14-3-3 C. lupus familiaris proteins YWHAE and YWHAQ, respectively.

Table 1. Claudins classified based on their interactome

Human claudins		Sequence similarity[a]	Permeability properties[b]	Interactome study			
				CoIP interactions	PRISMA complexes	Localization	Group
CLDN1		classic	anion barrier	61	proteasome	TJ	1
CLDN2		classic	cation pore	46	proteasome, CCT/TriC	TJ	1
CLDN3		classic	anion barrier	25	proteasome, CCT/TriC	TJ	1
CLDN4		classic	anion barrier	24	proteasome, CCT/TriC	TJ	1
CLDN5		classic	anion barrier	150	proteasome, CCT/TriC	TJ + cytosolic	2
CLDN6		classic	anion barrier	28	proteasome, CCT/TriC	TJ	1
CLDN7		classic	cation barrier/anion pore	30	proteasome	TJ	1
CLDN8		classic	anion barrier	43	proteasome	TJ	1
CLDN9		classic	anion barrier	107	proteasome, CCT/TriC	TJ + cytosolic	2
CLDN10b		classic	cation pore	200	proteasome, CCT/TriC	TJ + cytosolic	2
CLDN11		non-classic	anion barrier	90	no	TJ + cytosolic	4
CLDN12		non-classic		193	no	TJ + cytosolic	4
CLDN14		classic	anion barrier	146	no	TJ + cytosolic	4
CLDN15		classic	cation pore	250	no	TJ + cytosolic	4
CLDN16		non-classic	cation pore	41	no	TJ	3
CLDN17		classic	anion pore	NA	no	NA	NA
CLDN18	18.1	non-classic		161	proteasome	TJ + cytosolic	2
	18.2	non-classic	anion barrier	113	proteasome	TJ	1
CLDN19	19A	classic	cation barrier	36	no	TJ	3
	19B	classic	cation barrier	163	no	TJ + cytosolic	4
CLDN20		non-classic		137	no	TJ + cytosolic	4
CLDN22		non-classic		51	no	TJ	3
CLDN23		non-classic		175	proteasome, CCT/TriC	TJ + cytosolic	2
CLDN24		non-classic		82	no	TJ + cytosolic	4
CLDN25		non-classic		NA	no	NA	NA

Previous claudin classifications based on sequence similarity and permeability properties respectively, followed by the groups proposed in this study derived from the interactome data.
[a]Krause et al. (2008).
[b]Günzel and Yu (2013).

protein [Aip1]), involved in the assembly and maintenance of apical cell junctions in epithelial cells by regulating the F-actin dynamics (Lechuga et al., 2015). Looking at the pre-filtered PRISMA significant interacting proteins (Table S1C), other WD-repeat proteins were also found, such as G-protein subunits beta 1 (GNB1), GNB2, receptor of activated protein C kinase 1 (RACK1), the coatomer subunits alpha and beta (COPA, COPB2), actin-related protein 2/3 complex subunit 1B (ARPC1B), the eukaryotic translation initiation factor 3 subunit I (EIF3I), the serine-threonine kinase receptor-associated protein (STRAP), and the histone-binding protein RBBP7. In summary, these findings suggest that, in the context of the TJs, both the proteasome (interacting with claudin-1 to -10, -18, and -23) and the CCT/TriC chaperonin complex (interacting with claudin-2, -3, -4, -5, -6, -9, -10, and -23) would use the cytosolic tail of some claudins as physical support for localized protein degradation and folding of newly synthesized cytosolic proteins, respectively, thus contributing to the fast turnover that regulates paracellular transport in epithelia and the dynamic apical junctional complex formation and remodeling in response to physiological variations.

Additionally, seven members of the 14-3-3 protein family were found to interact with the cytosolic tail of some claudins. The 14-3-3 proteins are a family of highly conserved acidic proteins that can form homo- or heterodimers and interact with various cellular proteins in a phosphorylation-dependent or -independent manner. The molecular models of action for this protein family include clamping (stabilization of a certain conformation of the ligand), masking (blocking the access of another interacting protein), and scaffolding (recruiting additional proteins or molecules acting as a backbone for protein complex assembly). Some of the 14-3-3-binding proteins are involved in the regulation of the cytoskeleton, GTPase function, membrane signaling, and cell fate determination (Jin et al., 2004), and the interactions occur via motifs that often, but not always, include phosphorylated serine or threonine residues (Mrowiec and Schwappach, 2006). An *in silico* analysis of the cytosolic tail of claudins using the eukaryotic linear motif (ELM) resource (Kumar et al., 2019) predicted the interaction with 14-3-3 proteins through the canonical 14-3-3-binding phosphopeptide motif (LIG_1433_CanoR_1), present in 13 claudins (Table S2). However, the PRISMA dataset shows the phosphorylation-independent

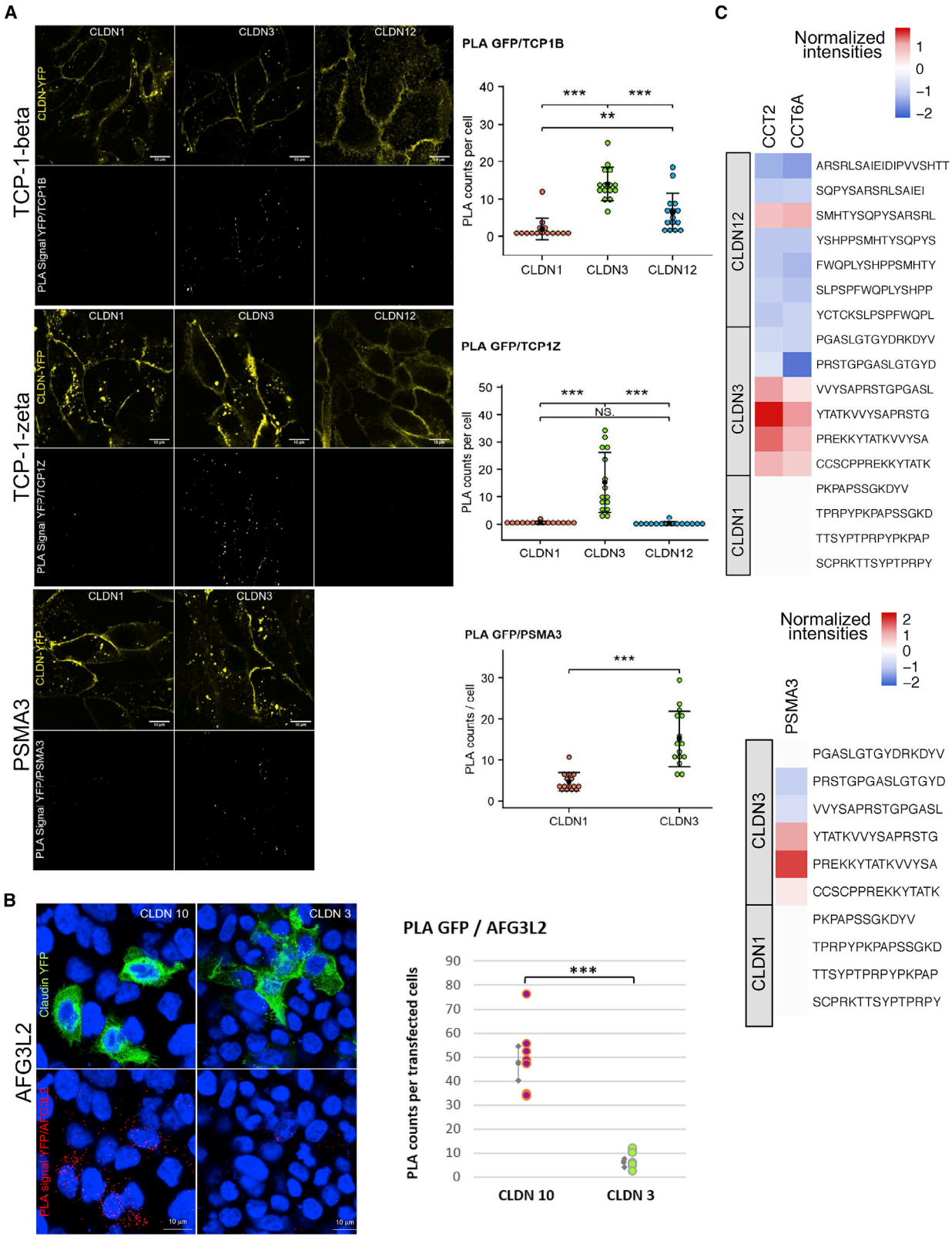

(legend on next page)

interaction of 14-3-3 proteins with unmodified peptides of at least five of those claudins (claudin-1, -7, -11, -16, -19A, and -23) and additional claudins with no predicted 14-3-3-binding motifs (claudin-2, -3, -4, -5, and -9).

The 14-3-3 protein family is known to be involved in membrane protein transport, and it could also be implicated in the targeting of claudins to the plasma membrane. However, comparing their PRISMA interaction patterns with the ones from the protein complexes previously discussed, it seems tentative to speculate that the different 14-3-3 isoforms could recruit the proteasome and the CCT/TRiC chaperonin complexes (as well as cytoskeletal proteins also identified by PRISMA) to the TJ.

PRISMA reveals phosphotyrosine-dependent interactions with the cytosolic C termini of claudins

In addition to mapping SLiM-based protein interactions of claudins, we also employed PRISMA to study the effect of PTMs on protein interactions of the cytosolic claudin tails. PTMs, particularly STY phosphorylations, regulate many aspects of the biology of claudins. Prediction studies on the different claudins forecast up to 10 possible phosphorylation sites, most located in the C-terminal cytosolic tail (González-Mariscal et al., 2010). Here, we focused on tyrosine phosphorylations described in the C-terminal PDZ domain-binding motif present in most claudins and defined by the dipeptide (Y-V-COOH), and residues in positions −3, −4, and −6 (Zhang et al., 2006). The C terminus of claudins interacts with the first PDZ domain of TJs protein ZO-1, -2, and -3 through the PDZ domain-binding motif, and this interaction is lost upon phosphorylation of tyrosine residues in positions −1 or −6 (Nomme et al., 2015) (Figure 5A). Therefore, when phosphorylated, the C terminus of claudins would be free to interact with other proteins. The disruption of the interaction between claudins and ZO proteins is part of the TJ remodeling process, an essential feature of this highly dynamic molecular suprastructure. Interestingly, the Tyr residue present at the position −1 of most claudins is a conserved putative Eph phosphorylation site (González-Mariscal et al., 2010), and the PhosphositePlus database (Hornbeck et al., 2015) shows that the tyrosine in position −1 of claudin-4 (Y208p) is phosphorylated by the Ephrin type-A receptor 2 (EphA2) tyrosine kinase. To study the effect of these phosphorylations, PTM-modified versions of C-terminal claudin peptides were designed with phospho-tyrosines in positions −1 or −6. Comparison of phosphorylated peptides with their unmodified counterparts using moderated t test identified PTM-specific interactors. We found 107 proteins differentially binding to 12 members of the claudin family, including proteins involved in internalization mechanisms (CLTC, DNM2, ANXA2, and S100A10) and endocytic sorting pathways (RAB6A, RAB1A, RAB11B, RAB7A, ARF6, and ARL8B).

In the case of claudins with phosphorylations described in tyrosine residues −1 and −6 (claudin-3, -5, and -6), the differences in the label-free quantification (LFQ) normalized intensity of proteins significantly binding to both modified peptides would translate into a difference in the binding strength depending on the position of the phosphorylated tyrosine residue (Figure 5B and Table S1D). Therefore, by using PRISMA, it is also possible to discriminate between the effects that two PTMs in close proximity have on the interaction with a specific protein.

DISCUSSION

In this study, we created an extended and comprehensive protein interaction map of human claudins using a combination of peptide-based (PRISMA) and full-length protein (coIP) interactomics. The catalog of interactions detected with coIPs includes known and novel interactors, with 758 proteins interacting with one or more members of the claudin family. This dataset serves as a resource for future studies focusing on the many different aspects of claudins, including their role as TJ proteins, implications in different cell-cell contact zones outside the TJs, processing in the ER, vesicular trafficking, turnover and degradation through different pathways, and non-canonical functions in nucleus and mitochondria.

PRISMA provided complementary protein interaction data that shed light on possible implications of the cytosolic disordered C-terminal region of claudins. Among the 148 significant interactors identified for these regions, we validated three groups of proteins that differentially bind to claudins: two protein complexes (proteasome and CCT/TRiC) and the 14-3-3 protein family. As tetraspan transmembrane proteins, claudins are synthesized and folded within the ER and typically degraded via the endo-lysosomal pathway. Therefore, the interaction with the two cytosolic protein complexes suggests an undescribed biological function for the C-terminal tail of claudins.

Spatially controlled protein translation and degradation are crucial in highly polarized cells allowing for a rapid response in regions where dynamic events occur. To maintain the steady-state of concentrated proteins necessary to create such subcellular domains, mRNA and protein complexes are either subjected to continuous active transport or anchored in place. For example, in dendritic spines of rat hippocampal neurons, the proteasome complex is sequestered by the actin cytoskeleton (Bingol and Schuman, 2006). Localized translation of ZO-1 and β-actin mRNAs in TJ and AJ, respectively, regulate cell adhesion (Nagaoka et al., 2012; Gutierrez et al., 2014), indicating that

Figure 4. PLAs confirm novel claudin interaction partners identified by PRISMA (CCT/TriC and proteasome subunits) and coIP (mitochondrial AFG3L2 protein)

(A) CCT/TRiC complex subunits beta and zeta (CCT2 and CCT6A) and proteasome subunit alpha 3 (PSMA3) interact with claudin-3 in MDCK-C7 cells, confirming the results from PRISMA (C) where these proteins showed an intensity profile that fits a SLiM-dependent type of interaction with this particular claudin but claudin-1 or -12. Dot plots represent the average number of PLA signals per cell.

(B) Immunofluorescence images of PLA between AFG3L2 and claudin-10 or claudin-3. For this experiment, Caco2 cells were transiently transfected with YFP-tagged claudin-10 or claudin-3. AFG3L2 mitochondrial protein interacts with claudin-10 but not with claudin-3. Almost no dots were visible in non-transfected cells. Dot plot representing the number of PLA signals per transfected cell. Results are statistically significant ($p < 0.05$) and confirm the results of the YFP-tagged claudin-10 coIP. The stars indicate the significance level (***p value of less than 0.001, **p value of less than 0.01).

CellPress
OPEN ACCESS

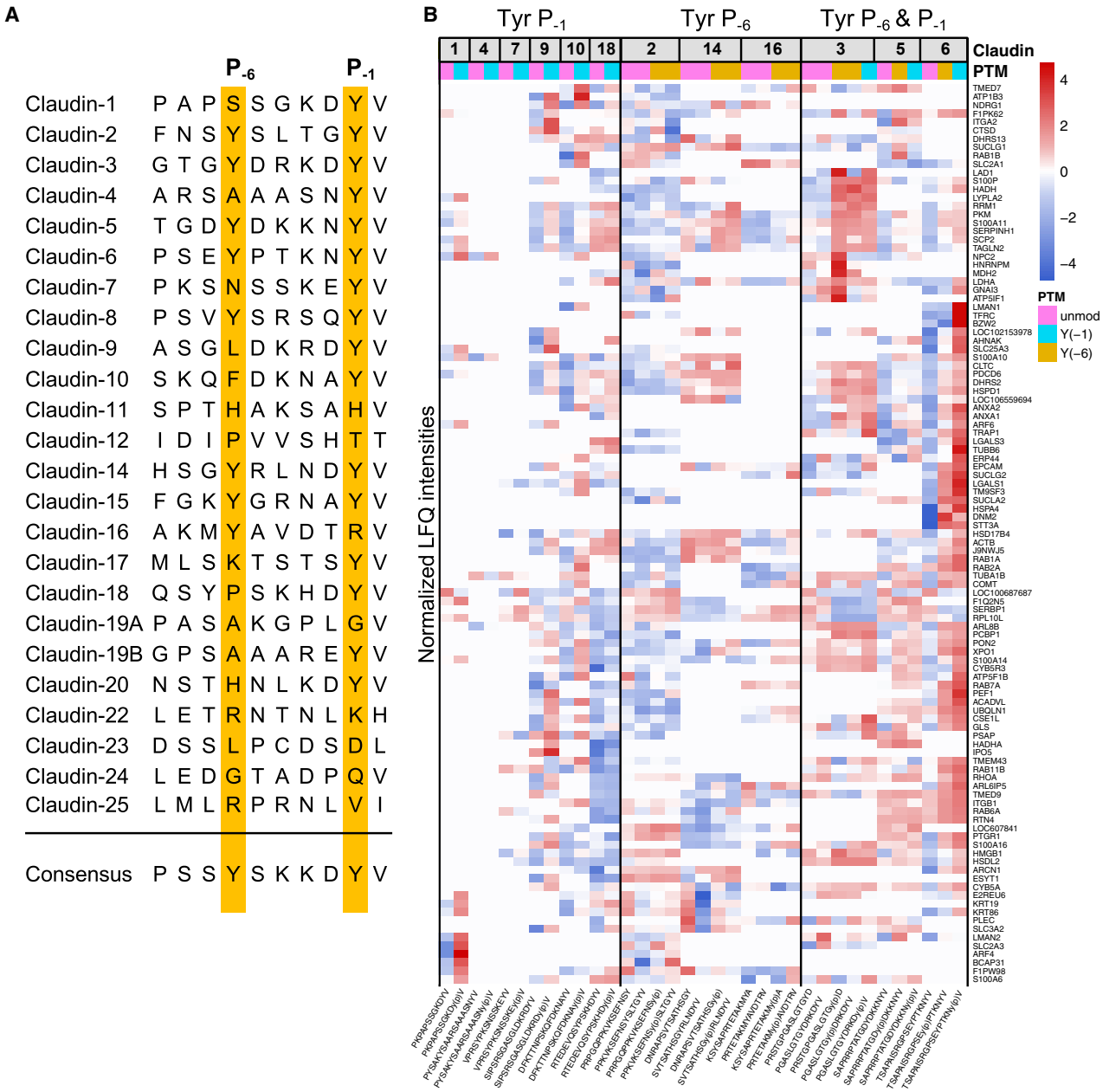

Figure 5. PRISMA shows interactions regulated by phosphorylation of the non-canonical PDZ domain-binding motif of claudins and different effects of PTMs located in close proximity

(A) Sequence alignment of the last 10 amino acids in human claudins where the non-canonical PDZ domain-binding motif is located. Tyrosine residues often occupy positions designated as −1 and −6 in human claudins (highlighted in yellow).

(B) Interactions identified for claudins with one or two tyrosine residues as phosphoacceptor sites. Proteins interacting with the phosphorylated peptides show different LFQ intensity values depending on the position of the PTM. Only the interactor AHNAK nucleoprotein (AHNAK) contains a PDZ domain.

spatially controlled biological processes also take place in the cell junctions of epithelial cells. Considering the previous evidence, the identification by PRISMA, and subsequent confirmation of the interaction between the cytosolic tail of some claudins and the CCT/TRiC chaperonin and proteasome complexes, we hypothesize that localized protein folding and protein degradation by the proteasome also occur in TJs. The cytosolic tails of certain claudins would therefore act as a scaffold facilitating a contact point for the protein complexes involved, and 14-3-3 and other proteins might mediate these interactions (Figure 6).

Additionally, PRISMA revealed interactions between claudins and other proteins involved in their internalization, sorting, and degradation at the PDZ domain-binding motif. These interactions are also differentially regulated by phosphorylation of the

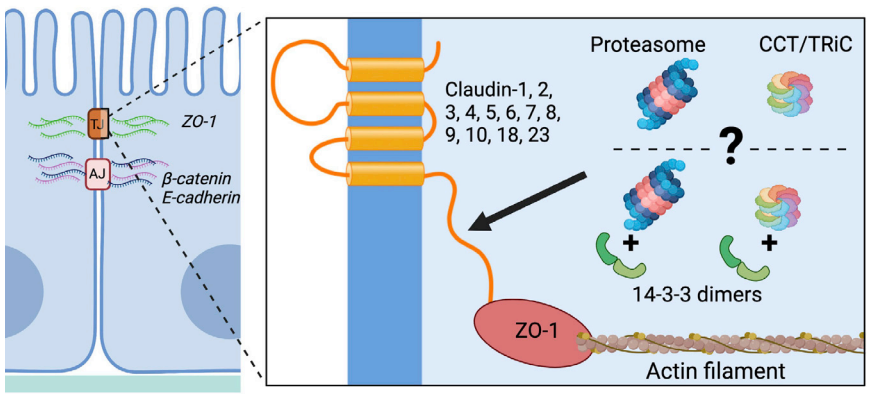

Figure 6. Introduction of the hypothesis derived from the PRISMA results

Evidence of spatially localized mRNA coding TJ and AJ proteins in epithelial cells (Gutierrez et al., 2014; Nagaoka et al., 2012) in combination with our PRISMA results point to the C-terminal tails of some claudins as a scaffold for localized biological processes such as protein folding and protein degradation mediated by the proteasome. We also speculate that 14-3-3 proteins could possibly facilitate these interactions, although our data are not conclusive in this regard. Created with BioRender.com.

tyrosines in positions −1 and −6. Phosphorylation of these residues not only disrupts the interaction with PDZ domain-containing proteins, such as TJs protein ZO-1, -2, or -3, and leads to the internalization of some claudins but also allows the PDZ domain-binding motif to differentially interact with other proteins depending on the modified site.

Claudins have previously been classified into subgroups based on different criteria such as sequence similarity (Krause et al., 2008) or functionality based on biochemical properties of the extracellular loops and their physiological role within the TJ (Günzel and Yu, 2013). Here, we propose an alternative classification of claudins into four groups based on the pan-claudin family interactome data. Our data show two subgroups of claudins based on the interaction with cytosolic protein complexes through their C-terminal tails (claudin-1 to -10, -18, and -23), indicating possible biological implications of these claudins outside the canonical TJ-associated roles. Based on the microscopy and coIP results, we observed two additional subgroups of claudins regarding their localization in the cell, which is either restricted to the TJs or also present in cytosol, most likely in vesicles according to the identified interacting proteins (Table 1).

Combining the complementary information obtained from two orthogonal pull-down-based proteomics techniques generates the first comprehensive interactome landscape of the pan-claudin protein family. Interacting proteins from different cell compartments can now be connected to individual members of the claudin family and different possible functions. The identification of protein complexes interacting with the unstructured cytosolic tail of specific claudins by PRISMA leads to the hypothesis of their possible implication in localized biological processes in epithelial cells. PRISMA also provided information about interactions with the PDZ domain-binding motif of claudins regulated by phosphorylation. The pan-claudin family interactome allows for a better understanding of claudins and their implication in several processes within the cell. It serves as a resource for future studies related to the many aspects of their biology inside and outside the TJs, as well as their role in the various pathologies they are related to.

Limitations of the study

This study uses the combination of recombinant claudin proteins carrying an epitope tag and a peptide array-based interaction experiment to unravel the claudin interactome. While the immunoprecipitation-based claudin interactome is based on full-length protein pull-downs, it is biased toward the identification of high-affinity interactions, which can survive the precipitation conditions. The PRISMA method allows the identification of motif-based interactions that are frequently of low affinity. As the PRISMA analysis was focused on the C-terminal part of the proteins, it lacks low-affinity interactions of the N-terminal parts. In general, this study provides a comprehensive overview of the claudin families' interactions with a focus on the regulatorily important C terminus. The experiments in this study were carried out using the MDCK-C7 cell line, a subtype cloned from the heterogeneous MDCK parental cell line, a prototypical polarized epithelial cell line widely used to study epithelial development and function, and one of the few immortalized renal epithelial cells, established by Madin and Darby in 1958 and characterized for the first time in 1966 (Gaush et al., 1966). The MDCK-C7 cell line shares properties with the MDCK I high-resistance subtype (high transepithelial resistance and very tight TJs) and resembles the principal cells (PCs) of the renal collecting duct involved in K+ secretion and Na+ reabsorption (Gekle et al., 1994). Therefore, some interactions described in this study might be directly connected to the characteristics of this particular phenotype.

STAR★METHODS

Detailed methods are provided in the online version of this paper and include the following:

- KEY RESOURCES TABLE
- RESOURCE AVAILABILITY
  - Lead contact
  - Materials availability
  - Data and code availability
- EXPERIMENTAL MODEL AND SUBJECT DETAILS
  - MDCK C7 cells
  - Caco2 cells
- METHOD DETAILS
  - Stable MDCK-C7 claudin cell lines generation
  - Transient transfection of Caco2 cells
  - IF staining for confocal microscopy
  - Western blotting

- Co-immunoprecipitations (CoIP)
- On-bead protein digestion
- Peptide clean-up
- LC-MS/MS
- PRISMA experiments
- PRISMA pull-downs
- In solution protein digestion
- Peptide clean-up
- LC-MS/MS
- Proximity ligation assays

- QUANTIFICATION AND STATISTICAL ANALYSIS
  - MS data processing with MaxQuant
  - Statistical analysis of MS data
  - CoIP data
  - PRISMA data
  - GO annotations and enrichment analysis

SUPPLEMENTAL INFORMATION

Supplemental information can be found online at https://doi.org/10.1016/j.celrep.2022.111588.

ACKNOWLEDGMENTS

L.S.-A. was supported by a BIH (Berlin Institute of Health, Berlin, Germany) translational PhD project grant to D.M. and G.D. E.R. was supported by a BSIO fellowship. A.L. was supported by the FNR (Fond National de Recherche, Luxembourg) PEARL CPIL grant to G.D. We thank Dr. Dorothee Günzel for the claudin plasmids and Dr. Alexander Ludwig for discussions of the interactome data. We thank Dr. Anje Sporbert from the Advanced Light Microscopy facility and Dr. Hans-Peter Rahn from the Flow Cytometry platform at the MDC (Max-Delbrück Center, Berlin, Germany) for their technical support in this project.

AUTHOR CONTRIBUTIONS

L.S.-A. performed most of the experiments, cloning, microscopy, and data analysis, created the figures, and wrote the draft. E.R. and D.P. helped with the data analysis. U.R. provided access to the PRISMA peptide matrices. T.B. helped with the biological data interpretation. D.M. and G.D. conceptualized the project. A.L. helped with the data collection for the PRISMA screen. R.G. and S.R. performed the PLA experiments. H.G. collected microscope images for the manuscript. D.M., P.M., and G.D. secured funding and supervised the project. L.S.-A. and G.D. wrote the final manuscript.

DECLARATION OF INTERESTS

The authors declare no competing interests.

Received: January 28, 2022
Revised: July 4, 2022
Accepted: October 11, 2022
Published: November 8, 2022

REFERENCES

Bingol, B., and Schuman, E.M. (2006). Activity-dependent dynamics and sequestration of proteasomes in dendritic spines. Nature *441*, 1144–1148. https://doi.org/10.1038/nature04769.

Cai, J., Culley, M.K., Zhao, Y., and Zhao, J. (2018). The role of ubiquitination and deubiquitination in the regulation of cell junctions. Protein Cell *9*, 754–769. https://doi.org/10.1007/s13238-017-0486-3.

Chen, C.-J., Ou, Y.-C., Li, J.-R., Chang, C.-Y., Pan, H.-C., Lai, C.-Y., Liao, S.-L., Raung, S.-L., and Chang, C.-J. (2014). Infection of pericytes in vitro by Japanese encephalitis virus disrupts the integrity of the endothelial barrier. J. Virol. *88*, 1150–1161. https://doi.org/10.1128/JVI.02738-13.

Cornish, J., Chamberlain, S.G., Owen, D., and Mott, H.R. (2020). Intrinsically disordered proteins and membranes: a marriage of convenience for cell signalling? Biochem. Soc. Trans. *48*, 2669–2689. https://doi.org/10.1042/BST20200467.

Coyne, C.B., Gambling, T.M., Boucher, R.C., Carson, J.L., and Johnson, L.G. (2003). Role of claudin interactions in airway tight junctional permeability. Am. J. Physiol. Lung Cell Mol. Physiol. *285*, L1166–L1178. https://doi.org/10.1152/ajplung.00182.2003.

Cuevas, M.E., Gaska, J.M., Gist, A.C., King, J.M., Sheller, R.A., and Todd, M.C. (2015). Estrogen-dependent expression and subcellular localization of the tight junction protein claudin-4 in HEC-1A endometrial cancer cells. Int. J. Oncol. *47*, 650–656. https://doi.org/10.3892/ijo.2015.3030.

Daugherty, B.L., Ward, C., Smith, T., Ritzenthaler, J.D., and Koval, M. (2007). Regulation of heterotypic claudin compatibility. J. Biol. Chem. *282*, 30005–30013. https://doi.org/10.1074/jbc.M703547200.

De Benedetto, A., Rafaels, N.M., McGirt, L.Y., Ivanov, A.I., Georas, S.N., Cheadle, C., Berger, A.E., Zhang, K., Vidyasagar, S., Yoshida, T., et al. (2011). Tight junction defects in atopic dermatitis. J. Allergy Clin. Immunol. *127*, 773–786, e7. https://doi.org/10.1016/j.jaci.2010.10.018.

Dhawan, P., Singh, A.B., Deane, N.G., No, Y., Shiou, S.-R., Schmidt, C., Neff, J., Washington, M.K., and Beauchamp, R.D. (2005). Claudin-1 regulates cellular transformation and metastatic behavior in colon cancer. J. Clin. Invest. *115*, 1765–1776. https://doi.org/10.1172/JCI24543.

Dittmar, G., Hernandez, D.P., Kowenz-Leutz, E., Kirchner, M., Kahlert, G., Wesolowski, R., Baum, K., Knoblich, M., Hofstätter, M., Muller, A., et al. (2019). PRISMA: protein interaction screen on peptide matrix reveals interaction footprints and modifications- dependent interactome of intrinsically disordered C/EBPβ. iScience *13*, 351–370. https://doi.org/10.1016/j.isci.2019.02.026.

Evans, M.J., von Hahn, T., Tscherne, D.M., Syder, A.J., Panis, M., Wölk, B., Hatziioannou, T., McKeating, J.A., Bieniasz, P.D., and Rice, C.M. (2007). Claudin-1 is a hepatitis C virus co-receptor required for a late step in entry. Nature *446*, 801–805. https://doi.org/10.1038/nature05654.

Frank, R. (1992). Spot-synthesis: an easy technique for the positionally addressable, parallel chemical synthesis on a membrane support. Tetrahedron *48*, 9217–9232. https://doi.org/10.1016/S0040-4020(01)85612-X.

Gaush, C.R., Hard, W.L., and Smith, T.F. (1966). Characterization of an Established Line of Canine Kidney Cells (MDCK). Proceedings of the Society for Experimental Biology and Medicine. *122*, 931–935. https://doi.org/10.3181/00379727-122-31293.

Gekle, M., Wünsch, S., Oberleithner, H., and Silbernagl, S. (1994). Characterization of two MDCK-cell subtypes as a model system to study principal cell and intercalated cell properties. Pflugers Arch. *428*, 157–162. https://doi.org/10.1007/BF00374853.

Gomes, I., Sierra, S., and Devi, L.A. (2016). Detection of receptor heteromerization using in situ proximity ligation assay. Curr. Protoc. Pharmacol. *75*, 2, 16. 31. https://doi.org/10.1002/cpph.15.

González-Mariscal, L., Garay, E., and Quirós, M. (2010). Chapter 6 - regulation of claudins by posttranslational modifications and cell-signaling cascades. In Current Topics in Membranes, A.S.L. Yu, ed. (Academic Press), pp. 113–150. https://doi.org/10.1016/S1063-5823(10)65006-5.

Günzel, D., and Yu, A.S.L. (2013). Claudins and the modulation of tight junction permeability. Physiol. Rev. *93*, 525–569. https://doi.org/10.1152/physrev.00019.2012.

Gutierrez, N., Eromobor, I., Petrie, R.J., Vedula, P., Cruz, L., and Rodriguez, A.J. (2014). The β-actin mRNA zipcode regulates epithelial adherens junction assembly but not maintenance. RNA *20*, 689–701. https://doi.org/10.1261/rna.043208.113.

Hagen, S.J. (2017). Non-canonical functions of claudin proteins: beyond the regulation of cell-cell adhesions. Tissue Barriers *5*, e1327839. https://doi.org/10.1080/21688370.2017.1327839.

Hegde, A.N. (2004). Ubiquitin-proteasome-mediated local protein degradation and synaptic plasticity. Progress in Neurobiology *73*, 311–357. https://doi.org/10.1016/j.pneurobio.2004.05.005.

Hein, M.Y., Hubner, N.C., Poser, I., Cox, J., Nagaraj, N., Toyoda, Y., Gak, I.A., Weisswange, I., Mansfeld, J., Buchholz, F., et al. (2015). A human interactome in three quantitative dimensions organized by stoichiometries and abundances. Cell *163*, 712–723. https://doi.org/10.1016/j.cell.2015.09.053.

Hernandez, D.P., and Dittmar, G. (2021). Peptide array–based interactomics. Anal. Bioanal. Chem. https://doi.org/10.1007/s00216-021-03367-8.

Hornbeck, P.V., Zhang, B., Murray, B., Kornhauser, J.M., Latham, V., and Skrzypek, E. (2015). PhosphoSitePlus, 2014: mutations, PTMs and recalibrations. Nucleic Acids Res. *43*, D512–D520. https://doi.org/10.1093/nar/gku1267.

Huang, D.W., Sherman, B.T., and Lempicki, R.A. (2009a). Systematic and integrative analysis of large gene lists using DAVID bioinformatics resources. Nat. Protoc. *4*, 44–57. https://doi.org/10.1038/nprot.2008.211.

Huang, D.W., Sherman, B.T., and Lempicki, R.A. (2009b). Bioinformatics enrichment tools: paths toward the comprehensive functional analysis of large gene lists. Nucleic Acids Res. *37*, 1–13. https://doi.org/10.1093/nar/gkn923.

Hubner, N.C., Bird, A.W., Cox, J., Splettstoesser, B., Bandilla, P., Poser, I., Hyman, A., and Mann, M. (2010). Quantitative proteomics combined with BAC TransgeneOmics reveals in vivo protein interactions. J. Cell Biol *189*, 739–754. https://doi.org/10.1083/jcb.200911091.

Iakoucheva, L.M., Radivojac, P., Brown, C.J., O'Connor, T.R., Sikes, J.G., Obradovic, Z., and Dunker, A.K. (2004). The importance of intrinsic disorder for protein phosphorylation. Nucleic Acids Res. *32*, 1037–1049. https://doi.org/10.1093/nar/gkh253.

Ikari, A., Watanabe, R., Sato, T., Taga, S., Shimobaba, S., Yamaguchi, M., Yamazaki, Y., Endo, S., Matsunaga, T., and Sugatani, J. (2014). Nuclear distribution of claudin-2 increases cell proliferation in human lung adenocarcinoma cells. Biochim. Biophys. Acta *1843*, 2079–2088. https://doi.org/10.1016/j.bbamcr.2014.05.017.

Ivarsson, Y., and Jemth, P. (2019). Affinity and specificity of motif-based protein-protein interactions. Curr. Opin. Struct. Biol. *54*, 26–33. https://doi.org/10.1016/j.sbi.2018.09.009.

Jin, J., Smith, F.D., Stark, C., Wells, C.D., Fawcett, J.P., Kulkarni, S., Metalnikov, P., O'Donnell, P., Taylor, P., Taylor, L., et al. (2004). Proteomic, functional, and domain-based analysis of in vivo 14-3-3 binding proteins involved in cytoskeletal regulation and cellular organization. Curr. Biol. *14*, 1436–1450. https://doi.org/10.1016/j.cub.2004.07.051.

Katahira, J., Sugiyama, H., Inoue, N., Horiguchi, Y., Matsuda, M., and Sugimoto, N. (1997). Clostridium perfringens enterotoxin utilizes two structurally related membrane proteins as functional receptors in vivo. J. Biol. Chem. *272*, 26652–26658. https://doi.org/10.1074/jbc.272.42.26652.

Keilhauer, E.C., Hein, M.Y., and Mann, M. (2015). Accurate protein complex retrieval by affinity enrichment mass spectrometry (AE-MS) rather than affinity purification mass spectrometry (AP-MS). Mol. Cell. Proteomics *14*, 120–135. https://doi.org/10.1074/mcp.M114.041012.

Klepper, J., Wang, D., Fischbarg, J., Vera, J.C., Jarjour, I.T., O'Driscoll, K.R., and De Vivo, D.C. (1999). Defective glucose transport across brain tissue barriers: a newly recognized neurological syndrome. Neurochem. Res. *24*, 587–594. https://doi.org/10.1023/a:1022544131826.

Konrad, M., Schaller, A., Seelow, D., Pandey, A.V., Waldegger, S., Lesslauer, A., Vitzthum, H., Suzuki, Y., Luk, J.M., Becker, C., et al. (2006). Mutations in the tight-junction gene claudin 19 (CLDN19) are associated with renal magnesium wasting, renal failure, and severe ocular involvement. Am. J. Hum. Genet. *79*, 949–957. https://doi.org/10.1086/508617.

Kosugi, S., Hasebe, M., Tomita, M., and Yanagawa, H. (2009). Systematic identification of cell cycle-dependent yeast nucleocytoplasmic shuttling proteins by prediction of composite motifs. Proc. Natl. Acad. Sci. USA *106*, 10171–10176. https://doi.org/10.1073/pnas.0900604106.

Kozan, P.A., McGeough, M.D., Peña, C.A., Mueller, J.L., Barrett, K.E., Marchelletta, R.R., and Sivagnanam, M. (2015). Mutation of EpCAM leads to intestinal barrier and ion transport dysfunction. J. Mol. Med. (Berl.) *93*, 535–545. https://doi.org/10.1007/s00109-014-1239-x.

Krause, G., Winkler, L., Mueller, S.L., Haseloff, R.F., Piontek, J., and Blasig, I.E. (2008). Structure and function of claudins. Biochim. Biophys. Acta Biomembr. *1778*, 631–645. https://doi.org/10.1016/j.bbamem.2007.10.018.

Kumar, M., Gouw, M., Michael, S., Sámano-Sánchez, H., Pancsa, R., Glavina, J., Diakogianni, A., Valverde, J.A., Bukirova, D., Čalyševa, J., et al. (2019). ELM—the eukaryotic linear motif resource in 2020. Nucleic Acids Res.Gkz1030 https://doi.org/10.1093/nar/gkz1030.

Kyuno, D., Takasawa, A., Kikuchi, S., Takemasa, I., Osanai, M., and Kojima, T. (2021). Role of tight junctions in the epithelial-to-mesenchymal transition of cancer cells. Biochim. Biophys. Acta Biomembr. *1863*, 183503. https://doi.org/10.1016/j.bbamem.2020.183503.

Ladwein, M., Pape, U.F., Schmidt, D.S., Schnölzer, M., Fiedler, S., Langbein, L., Franke, W.W., Moldenhauer, G., and Zöller, M. (2005). The cell-cell adhesion molecule EpCAM interacts directly with the tight junction protein claudin-7. Exp. Cell Res. *309*, 345–357. https://doi.org/10.1016/j.yexcr.2005.06.013.

Lechuga, S., Baranwal, S., and Ivanov, A.I. (2015). Actin-interacting protein 1 controls assembly and permeability of intestinal epithelial apical junctions. Am. J. Physiol. Gastrointest. Liver Physiol. *308*, G745–G756. https://doi.org/10.1152/ajpgi.00446.2014.

Lee, J.-W., Hsiao, W.-T., Chen, H.-Y., Hsu, L.-P., Chen, P.-R., Lin, M.-D., Chiu, S.-J., Shih, W.-L., and Hsu, Y.-C. (2010). Upregulated claudin-1 expression confers resistance to cell death of nasopharyngeal carcinoma cells. Int. J. Cancer *126*, 1353–1366. https://doi.org/10.1002/ijc.24857.

Li, D., and Roberts, R. (2001). Human Genome and Diseases: Review *58*, 13.

Liu, F., Koval, M., Ranganathan, S., Fanayan, S., Hancock, W.S., Lundberg, E.K., Beavis, R.C., Lane, L., Duek, P., McQuade, L., et al. (2016). Systems proteomics view of the endogenous human claudin protein family. J. Proteome Res. *15*, 339–359. https://doi.org/10.1021/acs.jproteome.5b00769.

Mandel, I., Paperna, T., Volkowich, A., Merhav, M., Glass-Marmor, L., and Miller, A. (2012). The ubiquitin–proteasome pathway regulates claudin 5 degradation. J. Cell. Biochem. *113*, 2415–2423. https://doi.org/10.1002/jcb.24118.

Meyer, K., Kirchner, M., Uyar, B., Cheng, J.-Y., Russo, G., Hernandez-Miranda, L.R., Szymborska, A., Zauber, H., Rudolph, I.-M., Willnow, T.E., et al. (2018). Mutations in disordered regions can cause disease by creating dileucine motifs. Cell *175*, 239–253, e17. https://doi.org/10.1016/j.cell.2018.08.019.

Milatz, S., and Breiderhoff, T. (2017). One gene, two paracellular ion channels—claudin-10 in the kidney. Pflugers Arch - Eur J Physiol *469*, 115–121. https://doi.org/10.1007/s00424-016-1921-7.

Milatz, S., Himmerkus, N., Wulfmeyer, V.C., Drewell, H., Mutig, K., Hou, J., Breiderhoff, T., Müller, D., Fromm, M., Bleich, M., and Günzel, D. (2017). Mosaic expression of claudins in thick ascending limbs of Henle results in spatial separation of paracellular Na^+ and Mg^{2+} transport. Proc. Natl. Acad. Sci. USA *114*, E219–E227. https://doi.org/10.1073/pnas.1611684114.

Morita, K., Furuse, M., Fujimoto, K., and Tsukita, S. (1999). Claudin multigene family encoding four-transmembrane domain protein components of tight junction strands. Proc. Natl. Acad. Sci. USA *96*, 511–516. https://doi.org/10.1073/pnas.96.2.511.

Mrowiec, T., and Schwappach, B. (2006). 14-3-3 proteins in membrane protein transport. Biol. Chem. *387*. https://doi.org/10.1515/BC.2006.152.

Nagaoka, K., Udagawa, T., and Richter, J.D. (2012). CPEB-mediated ZO-1 mRNA localization is required for epithelial tight-junction assembly and cell polarity. Nat. Commun. *3*, 675. https://doi.org/10.1038/ncomms1678.

Nomme, J., Antanasijevic, A., Caffrey, M., Van Itallie, C.M., Anderson, J.M., Fanning, A.S., and Lavie, A. (2015). Structural basis of a key factor regulating the affinity between the zonula occludens first PDZ domain and claudins. J. Biol. Chem. *290*, 16595–16606. https://doi.org/10.1074/jbc.M115.646695.

Oshima, T., Miwa, H., and Joh, T. (2008). Changes in the expression of claudins in active ulcerative colitis. J. Gastroenterol. Hepatol. *23*, S146–S150. https://doi.org/10.1111/j.1440-1746.2008.05405.x.

Perkins, J.R., Diboun, I., Dessailly, B.H., Lees, J.G., and Orengo, C. (2010). Transient protein-protein interactions: structural, functional, and network properties. Structure *18*, 1233–1243. https://doi.org/10.1016/j.str.2010.08.007.

Prado Martins, R., Findakly, S., Daskalogianni, C., Teulade-Fichou, M.-P., Blondel, M., and Fåhraeus, R. (2018). In cellulo protein-mRNA interaction assay to determine the action of G-quadruplex-binding molecules. Molecules *23*, 3124. https://doi.org/10.3390/molecules23123124.

Ramberger, E., Sapozhnikova, V., Kowenz-Leutz, E., Zimmermann, K., Nicot, N., Nazarov, P.V., Perez-Hernandez, D., Reimer, U., Mertins, P., Dittmar, G., and Leutz, A. (2021a). PRISMA and BioID disclose a motifs-based interactome of the intrinsically disordered transcription factor C/EBPα. iScience *24*, 102686. https://doi.org/10.1016/j.isci.2021.102686.

Ramberger, E., Suarez-Artiles, L., Perez-Hernandez, D., Haji, M., Popp, O., Reimer, U., Leutz, A., Dittmar, G., and Mertins, P. (2021b). A universal peptide matrix interactomics approach to disclose motif-dependent protein binding. Mol. Cell. Proteomics *20*, 100135. https://doi.org/10.1016/j.mcpro.2021.100135.

Rappsilber, J., Ishihama, Y., and Mann, M. (2003). Stop and Go extraction tips for matrix-assisted laser desorption/ionization, nanoelectrospray, and LC/MS sample pretreatment in proteomics. Anal. Chem. *75*, 663–670. https://doi.org/10.1021/ac026117i.

Schreiber, E., Matthias, P., Müller, M.M., and Schaffner, W. (1989). Rapid detection of octamer binding proteins with "mini-extracts", prepared from a small number of cells. Nucleic Acids Res *17*, 6419.

Stein, A., and Aloy, P. (2008). Contextual specificity in peptide-mediated protein interactions. PLoS One *3*, e2524. https://doi.org/10.1371/journal.pone.0002524.

Sun, Z.-Y., Wei, J., Xie, L., Shen, Y., Liu, S.-Z., Ju, G.-Z., Shi, J.-P., Yu, Y.-Q., Zhang, X., Xu, Q., and Hemmings, G.P. (2004). The CLDN5 locus may be involved in the vulnerability to schizophrenia. Eur. Psychiatr. *19*, 354–357. https://doi.org/10.1016/j.eurpsy.2004.06.007.

Tan, B., Yatim, S.M.J.M., Peng, S., Gunaratne, J., Hunziker, W., and Ludwig, A. (2020). The mammalian crumbs complex defines a distinct polarity domain apical of epithelial tight junctions. Curr. Biol. *30*, 2791–2804, e6. https://doi.org/10.1016/j.cub.2020.05.032.

Thorens, B., Lodish, H.F., and Brown, D. (1990). Differential localization of two glucose transporter isoforms in rat kidney. Am. J. Physiol. *259*, C286–C294. https://doi.org/10.1152/ajpcell.1990.259.2.C286.

Thorleifsson, G., Holm, H., Edvardsson, V., Walters, G.B., Styrkarsdottir, U., Gudbjartsson, D.F., Sulem, P., Halldorsson, B.V., de Vegt, F., d'Ancona, F.C.H., et al. (2009). Sequence variants in the CLDN14 gene associate with kidney stones and bone mineral density. Nat. Genet. *41*, 926–930. https://doi.org/10.1038/ng.404.

Todd, M.C., Petty, H.M., King, J.M., Piana Marshall, B.N., Sheller, R.A., and Cuevas, M.E. (2015). Overexpression and delocalization of claudin-3 protein in MCF-7 and MDA-MB-415 breast cancer cell lines. Oncol. Lett. *10*, 156–162. https://doi.org/10.3892/ol.2015.3160.

Tompa, P., Davey, N.E., Gibson, T.J., and Babu, M.M. (2014). A million peptide motifs for the molecular biologist. Mol. Cell *55*, 161–169. https://doi.org/10.1016/j.molcel.2014.05.032.

Towbin, H., Staehelin, T., and Gordon, J. (1979). Electrophoretic transfer of proteins from polyacrylamide gels to nitrocellulose sheets: procedure and some applications *79*, 4350–4354. https://doi.org/10.1073/pnas.76.9.4350.

Traweger, A., Fang, D., Liu, Y.-C., Stelzhammer, W., Krizbai, I.A., Fresser, F., Bauer, H.-C., and Bauer, H. (2002). The tight junction-specific protein occludin is a functional target of the E3 ubiquitin-protein ligase itch. J. Biol. Chem. *277*, 10201–10208. https://doi.org/10.1074/jbc.M111384200.

Vallon, V. (2020). Glucose transporters in the kidney in health and disease. Pflugers Arch - Eur J Physiol *472*, 1345–1370. https://doi.org/10.1007/s00424-020-02361-w.

Weber, S., Hoffmann, K., Jeck, N., Saar, K., Boeswald, M., Kuwertz-Broeking, E., Meij, I.I., Knoers, N.V., Cochat, P., Šuláková, T., et al. (2000). Familial hypomagnesaemia with hypercalciuria and nephrocalcinosis maps to chromosome 3q27 and is associated with mutations in the PCLN-1 gene. Eur. J. Hum. Genet. *8*, 414–422. https://doi.org/10.1038/sj.ejhg.5200475.

Zeissig, S., Burgel, N., Gunzel, D., Richter, J., Mankertz, J., Wahnschaffe, U., Kroesen, A.J., Zeitz, M., Fromm, M., and Schulzke, J.-D. (2007). Changes in expression and distribution of claudin 2, 5 and 8 lead to discontinuous tight junctions and barrier dysfunction in active Crohn's disease. Gut *56*, 61–72. https://doi.org/10.1136/gut.2006.094375.

Zhang, Y., Yeh, S., Appleton, B.A., Held, H.A., Kausalya, P.J., Phua, D.C.Y., Lee Wong, W., Lasky, L.A., Wiesmann, C., Hunziker, W., and Sidhu, S.S. (2006). Convergent and divergent ligand specificity among PDZ domains of the LAP and zonula occludens (ZO) families. J. Biol. Chem. *281*, 22299–22311. https://doi.org/10.1074/jbc.M602902200.

Zheng, A., Yuan, F., Li, Y., Zhu, F., Hou, P., Li, J., Song, X., Ding, M., and Deng, H. (2007). Claudin-6 and claudin-9 function as additional coreceptors for hepatitis C virus. J. Virol. *81*, 12465–12471. https://doi.org/10.1128/JVI.01457-07.

Zhou, Y., Zhou, B., Pache, L., Chang, M., Khodabakhshi, A.H., Tanaseichuk, O., Benner, C., and Chanda, S.K. (2019). Metascape provides a biologist-oriented resource for the analysis of systems-level datasets. Nat. Commun. *10*, 1523. https://doi.org/10.1038/s41467-019-09234-6.

Zwanziger, D., Badziong, J., Ting, S., Moeller, L.C., Schmid, K.W., Siebolts, U., Wickenhauser, C., Dralle, H., and Fuehrer, D. (2015). The impact of CLAUDIN-1 on follicular thyroid carcinoma aggressiveness. Endocr. Relat. Cancer *22*, 819–830. https://doi.org/10.1530/ERC-14-0502.

STAR★METHODS

KEY RESOURCES TABLE

REAGENT or RESOURCE	SOURCE	IDENTIFIER
Antibodies		
rabbit anti-ZO-1	Invitrogen	Cat# 61-7300, RRID: AB_2533938
anti-Rabbit Alexa Fluor® 647	Abcam	Cat# ab150075, RRID:AB_2752244
GFP-Trap®_A nanobodies	Chromotek	Cat# gta-100, RRID: AB_2631357
Actin	Abcam	Cat# ab179467, RRID:AB_2737344
histone H3	Abcam	Cat# ab1791, RRID:AB_302613
TCP-1 β (D-8) (CCT2)	Santa Cruz Biotechnology	Cat# sc-374152, RRID:AB_10917207
TCP1 Z (F-4) (CCT6A)	Santa Cruz Biotechnology	sc-514466
20S Proteasome α6 (C-5) (PSMA3)	Santa Cruz Biotechnology	Cat# sc-271187, RRID:AB_10608973
Goat anti-rabbit HRP	Abcam	Cat# ab6721, RRID:AB_955447
Chemicals, peptides, and recombinant proteins		
Acetonitrile (ACN, MeCN, LC-MS grade)	Honeywell Riedel de Haehn	34967
ammonium bicarbonate (ABC)	Roth	T871.2
Benzonase	millipore	70664-3
BSA	Serva	11926
cOmplete™ Mini	Roche	11836153001
DDM	Bio Vision	2036-1
DTT	Sigma	D0632
EDTA	Merck	1.08417.1000
Formic acid (FA)	Merck-Millipore	1.002640100
G418-BC	Biochrom	A 2912
Gentamicin	Gibco	15710049
Glycerol	Alpha Aesar	38988
Glycine	Roth	3908.2
HEPES	Serva	25245.04
IAA	Sigma	I1149
IGEPAL-CA-630	Sigma	I8896
KCl	Sigma	P9541
Lipofectamine™ 2000	Invitrogen	11668027
Methanol (MeOH, LC-MS grade)	Honeywell Riedel de Haehn	34966
$MgCl_2$	Ambion	AM9530
Modified trypsin, sequencing grade	Promega	V5113
NaCl	Roth	3957.1
PBS	Gibco	14190-094
Penicillin-Streptomycin solution 100X	Sigma	TMS-AB2-C
Poly-L-Lysine solution	Sigma	P8920-100ML
Ponceau S solution	Sigma	81462
ProLong® Gold Antifade liquid mountant	Life Technologies	P36934
Protein Interaction Screen on Peptide Matrix (PRISMA)	JPT	PRISMA
SDS-polyacrylamide gels (mini protean TGX)	Biorad	456-1095
Sep-Pak C18 96-well plates	Waters	SKU: 186003966
Serum-free DMEM	Gibco	41965062

(*Continued on next page*)

Continued

REAGENT or RESOURCE	SOURCE	IDENTIFIER
Skim milk	Sigma	70166
STAGE tips: 3M™ C18 Empore™ disks	CDS Analytical	2215
TFA	Merck/Millipore	1.08262.0100
Thiourea	Roth	HN37.2
Tris	Sigma	T4661
Triton X-100	Sigma	T8532
Tween 20	Sigma	93773
Urea	Sigma	U0631
yeast tRNA	Invitrogen	AM7119
Critical commercial assays		
Duolink® *in situ* PLA® probe anti-rabbit MINUS	Sigma-Aldrich	DUO92004
Duolink® *in situ* PLA® probe anti-rabbit PLUS	Sigma-Aldrich	DUO92002
Duolink® *in situ* PLA® red starter kit mouse/rabbit	Sigma-Aldrich	DUO92007
Pierce™ BCA protein assay kit	Thermo Fisher Scientific	23227
Pierce™ ECL	Thermo Scientific	32106
Deposited data		
Mass spectrometry proteomics data	ProteomeXchange	PXD031094
Experimental models: Cell lines		
MDCK-C7		RRID: CVCL_0423
Software and algorithms		
MaxQuant version 1.5.2.8	Max-Plank Institute of Biochemistry	https://maxquant.org/
R version 3.5.0		https://cran.r-project.org/
RStudio version 1.0.143		https://www.rstudio.com/
ProTIGY Shiny app	Broad Institute	https://github.com/broadinstitute/protigy
DAVID functional annotation tool	Huang et al., 2009a, 2009b	
Metascape	Zhou et al., 2019	
Other		
nanoEASE M/Z peptideBEH C18, 1.7 μm, 100 μm ID, 100 mm analytical column	Waters	186008796
Centrifuge adaptors	Glygen	5010-21514
Dionex Ultimate 3000 RSLCnano	Thermo Fisher Scientific	
Easy-nLC™ 1200 HPLC system	Thermo Fisher Scientific	
Q-Exactive HF mass spectrometer	Thermo Fisher Scientific	
Q-Exactive HF-X mass spectrometer	Thermo Fisher Scientific	
ReproSil-Pur C18 3 μm beads	Dr. Maisch	271118
nanoEase M/Z symmetry C18, 5 μm, 180 μm ID, 20 mm trap column	Waters	186008821
Mini Trans-Blot System	Bio-Rad	1703930

RESOURCE AVAILABILITY

Lead contact

Further information and requests for resources and reagents should be directed to the lead contact, Gunnar Dittmar (gunnar.dittmar@lih.lu).

Materials availability

MDCK-C7 claudin stable cell lines are deposited at the European Collection of Authenticated Cell Cultures (ECACC).

Data and code availability

- Mass spectrometry Proteomics data have been deposited at the ProteomeXchange Consortium via the PRIDE [1] partner repository with the dataset identifier PXD031094.
- This paper does not report original code.
- Any additional information required to reanalyze the data reported in this paper is available from the lead contact upon request.

EXPERIMENTAL MODEL AND SUBJECT DETAILS

MDCK C7 cells

Adult female spontaneously immortalized kidney cell line from *Canis lupus familiaris* (RRID: CVCL_0423). Cultured in a humidified incubator at 37°C, 5% CO_2 in DMEM medium supplemented with 10%FBS and 1% Penicillin/Streptomycin.

Caco2 cells

Cultured in DMEM medium supplemented with 20% FBS and 1% Penicillin/Streptomycin.

METHOD DETAILS

Stable MDCK-C7 claudin cell lines generation

For every claudin isoform-specific cell line, MDCK-C7 cells were seeded at low density (0.125 x10^6 cells/ml) on 6 cm dishes in supplemented DMEM (10%FBS, 1% Penicillin/Streptomycin). The next day, cells were transfected with the YFP-claudin construct using Lipofectamine 2000 (Invitrogen) following the manufacturer's protocol and leaving one non-transfected dish as a control. First, 6 μg of the DNA construct and 20 μL Lipofectamine 2000 were separately diluted in 500 μL of serum-free DMEM (Gibco) and incubated for 5 min at RT. Then, both dilutions were combined in one Eppendorf tube, gently mixed by inverting the tube, and incubated for another 30 min at RT. The mix was added to the cell dish drop-wise and cells were incubated overnight. After incubation, the cell medium was replaced by supplemented DMEM for 24h. Then, the cell medium was changed to supplemented DMEM containing G418 (1 mg/mL, Biochrom) for antibiotic selection. The cell medium was replaced every 2 days until the cells on the control plate died (approximately after one week). After antibiotic selection, cells were sorted by FACS to keep those with higher fluorescence signals. Sorted cells were cultured in supplemented DMEM containing 0.6 mg/mL G418 and 50 μg/mL Gentamicin for at least 12h to avoid contamination and then kept in supplemented DMEM containing 0.6 mg/mL on a T-25 flask until they were 100% confluent. Stable MDCK C7 cells overexpressing the YFP-tagged claudin isoform were then split into aliquots of approximately 1x10^6 cells/ml and stored until used for the CoIP experiments.

Transient transfection of Caco2 cells

Cells were seeded on glass slides in 24 well plates and transfected at 50% confluency with Lipofectamine 3000 (Invitrogen). Transfection was performed according to the manufacturer's instructions, using 50 μL of Opti-Mem medium, 0.5 μg of DNA (claudin-3, claudin-10, or claudin-23), 0.75 μL of Lipofectamine 3000 Reagent and 1 μL of P3000 Reagent per well, during 24h.

IF staining for confocal microscopy

MDCK stable cell lines were grown on Poly-L-lysine coated coverslips in 24-well cell culture plates for a standard immune staining protocol. Briefly, after reaching approximately 90% confluence cells were washed with PBS twice and fixed with 4% PFA. After washing with PBS (3 times, 5 min at RT), cells were permeabilized with 0.1% Triton X-100 in PBS (5 min at RT) and incubated in Blocking buffer (1% BSA 20mM Glycine in PBST (PBS with 0.1% Tween 20)) (30 min at RT). Coverslips were then carefully placed on top of parafilm in a humid chamber and incubated with the primary antibody (rabbit anti-ZO-1, 61–7300 Invitrogen) (1:400 in blocking buffer, 2h at RT or overnight at 4°C) followed by washing steps with PBST to remove the antibody excess (3 times 10 min each at RT). The incubation with the secondary antibody was again done in a humid chamber (anti-Rabbit Alexa Fluor 647, Abcam) (1:1000 in blocking buffer, 1h at RT) followed by more washing steps with PBST (3 times 10 min each at RT). For the counterstaining coverslips were incubated with DAPI (0.5 ug/ml, 1 min at RT), washed twice with PBS for 5 min at RT and once with ddH_2O, and mounted into a glass slide with a drop of ProLong Gold Antifade liquid mountant. Samples were stored at 4°C and protected from light.

Confocal imaging was performed with an LSM780 (Carl Zeiss Microscopy) and with a Leica SP8 TCS STED microscope (Leica Microsystems). For image acquisition with the LSM780, a PL APO DIC M27 63×/1.40 NA oil objective and two photomultipliers (PMTs) were used for detection. The system was controlled by Zeiss ZEN2010 software. An HC PL APO CS2 100×/1.40 NA oil objective and two hybrid detectors (HyDs) were used for image acquisition with the Leica SP8 TCS STED microscope. The system was controlled by Leica LAS X software.

Western blotting

As a quality control for the CoIP experiments aliquots from the input, non-bound fraction, and output were analyzed by western blotting. For the cell lysates used in PRISMA, immunoblotting was used to control the depletion of nuclei in the extracts. In both

cases, samples were mixed with 6x loading buffer and boiled for 5 min at 95°C, and then loaded into a 10–12% SDS-polyacrylamide gel and separated by electrophoresis at 100V in running buffer (25mM Tris, 200mM Glycine, 0.1% SDS, pH 8.3). Proteins were transferred to a nitrocellulose membrane with the Trans-Blot Turbo Midi System from Bio-Rad in Towbin running buffer (0.025M Tris, 0.192 M Glycine, pH 8.6, 20% methanol) (Towbin et al., 1979), at 100V for 1h. Successful transfer was confirmed by staining the membrane with Ponceau S solution for 5 min. The membrane was then rinsed with TBS-T (50mM Tris-HCl, 150mM NaCl, 0.1% Tween 20) to remove the remaining staining. Free binding sites in the membrane were blocked by incubation in 4% skim milk in TBS-T for 1h at RT and the membrane was then washed twice with TBS-T for 5 min at RT. For detection of actin, GFP/YFP/CFP expression for CoIPs, and histone H3 in the PRISMA cell extracts, membranes were incubated with the corresponding primary antibodies diluted in blocking solution overnight at 4°C (actin: ab179467, histone H3: ab1791, Abcam; GFP: Af1180, guinea-pig anti-GFP, Frontier Institute). Membranes were then washed 3 times for 5 min in TBS-T and incubated 1h at RT with an HRP-coupled secondary antibody raised against the species of the primary antibody. Membranes were washed 3x for 5 min in TBS-T, immersed in chemiluminescence reaction solution (Pierce ECL, Thermo Scientific) for 1 min. The chemiluminescence signal was detected by exposure to an autoradiography film in a dark room and developed with an auto processor. As expected, the highest GFP signal was detected in the output sample as a thick band with an approximate size between 49 and 59 kDa (depending on the claudin) or 27 kDa for the control cell line, indicating a successful immunoprecipitation of the recombinant claudin or the cytosolic GFP with the GFP-Trap_A nanobodies (Chromotek). In the MDCK C7 cell extracts used for PRISMA, a stronger band of approximately 17 kDa corresponding to histone H3 was detected in the precipitated nuclei sample a faint band of the same size was detected in the post-nuclear supernatant samples indicating an effective depletion of nuclear content in the cell lysates (data not shown).

Co-immunoprecipitations (CoIP)

Cell lysates for CoIP experiments

MDCK-C7 stable cell lines overexpressing YFP/CFP fused claudin isoforms or cytosolic eGFP were grown in 15 cm cell culture dishes in quadruplicates. Once they reached approximately 90% confluence they were ready to be harvested for cell lysis. After removing the cell medium, 15 cm dishes were placed on ice and washed twice with ice-cold PBS. Using a cell scraper, cells were gently detached from the culture dish, resuspended in PBS and collected into a pre-chilled 50 mL falcon tube, and spun down at 500x g for 5 min at 4°C, after removing the supernatant cell pellets were collected, snap-frozen, and stored at −80°C until the rest of the cell lines were grown and collected following the same procedure. For the cell lysate preparation, cell pellets were thawed on ice, resuspended in 1 mL cold PBS, and transferred to a pre-chilled 1.5 mL LoBind Eppendorf where cells were pelleted and resuspended in 400 μL of lysis buffer (150 mM NaCl, 50 mM Tris pH 7.5, 0.5 mM EDTA, 1% IGEPAL-CA-630, 5% Glycerol, cOmplete Mini protease inhibitor cocktail (Roche), and 1 μL/mL benzonase), passed through a 23G syringe needle and incubated on ice for 30 min. After the incubation, tubes were centrifuged at 18.000x g, for 10 min at 4°C to remove cell debris. The supernatant cell lysate was transferred to fresh pre-chilled tubes and kept on ice. A small aliquot was taken from each tube to estimate protein concentration by BCA (Pierce BCA Protein Assay Kit, ThermoFisher Scientific) following the manufacturer's protocol.

Pull-down using GFP-Trap nanobodies

CoIP experiments were done adapting the protocol from Hubner et al. (2010) to the GFP-Trap_A nanobodies (Chromotek) manufacturer's recommendations. After determination of the protein concentration, the volume equivalent to 1 mg of cell lysate was taken and brought up to 1 mL using dilution/wash (D/W) buffer (150 mM NaCl, 50 mM Tris pH 7.5, 0.5 mM EDTA, and 5% Glycerol) to obtain a cell lysate concentration of 1 mg/mL and a detergent final concentration lower than 0.4%. 50 μL of the diluted cell lysate were taken for further immunoblot analysis. In order to condition the nanobodies for the immunoprecipitation, 25 μL of GFP-Trap_A bead slurry were resuspended in ice-cold D/W buffer and spun down at 2.500xg for 4 min at 4°C, this step was done three times to ensure that the beads are properly washed. After removing the D/W buffer from the last washing step, the cell lysate was added to the equilibrated beads and incubated overnight at 4°C (in a cold room) under constant mixing on a rotator. After incubation, tubes were spun down at 2500 xg for 4 min at 4°C, 50 μL of the supernatant were taken for immunoblot analysis and the rest was removed. Beads were then washed as in previous steps but first with 500 μL of D/W buffer +0.05% IGEPAL-CA-630, then with 500 μL of D/W buffer without detergents, and last with 500 μL cold PBS. After centrifugation and removing the PBS from the last washing step, beads were snap-frozen and stored at −80°C until further on-bead protein digestion.

On-bead protein digestion

Frozen beads containing proteins from the CoIP experiments were thawed and incubated in 80μL urea/trypsin buffer (2M urea, 50 mM Tris pH 7.5, 1 mM DTT, and 5 μg/mL Trypsin) on a shaker (1h at 25°C, 1000 rpm). 80 μL of the supernatant were transferred to a fresh tube and beads were washed 2 more times with 60 μL of urea buffer (2M urea, 50 mM Tris pH 7.5). The on-bead digest and washes were combined in one tube with a total volume of 200, spun down at 5000 xg for 1 min to remove the leftover beads, and transfer to a fresh tube. Eluted proteins were reduced by adding 4 mM DTT (30 min incubation on a shaker at 25°C, 1000 rpm), and subsequently alkylated by adding 10 mM iodoacetamide (IAA) (45 min incubation on a shaker at 25°C, 1000 rpm, protected from light). Protein digestion was done by adding 0.5 μg of trypsin and incubating overnight (25°C on a shaker, 700 rpm).

Peptide clean-up

After overnight digestion with trypsin, samples were acidified adding 1% FA to reach a pH < 3 for further C18 STAGE tips (STop And Go Extraction tips) desalting (Rappsilber et al., 2003). Stage tips were prepared by packing two disks of Empore 3M C18 material into 200 μL pipette tips. Stage tips were placed in a centrifuge on 2 mL tubes using Glygen centrifuge adaptors, then washed and equilibrated by sequentially passing through 100 μL of MeOH (2 times), 100 μL of 50% ACN/0.1% FA, and 100 μL of 0.1% FA (2 times); for each step, stage tips were centrifuged at 3000 xg for 3 min, and 2mL tubes were exchanged after collecting 300 μL. After the washing and equilibrating steps, acidified digests were loaded into the stage tips with the same centrifugation conditions. At this step, acidified peptides were bound to the C18 material. Stage tips were then washed twice with 100 μL 0.1% FA to remove the remaining salts from the digestion. Desalted peptides were eluted into fresh tubes with 60 μL of 50% ACN/0.1% FA, and eluates were transferred to a 96-well measuring plate. Samples were snap-frozen, lyophilized in a speed vac, and stored at - 80°C until measured by LC-MS/MS.

LC-MS/MS

Dried, desalted peptides were reconstituted in 8 μL of MS sample buffer (3% ACN/0.1% FA.) and separated online with an Easy-nLC 1200 coupled to a Q-Exactive HF-X mass spectrometer equipped with an orbitrap electrospray ion source (Thermo Fisher Scientific). Samples were separated on a 20cm reverse-phase column packed in house with 3 μm C18-Reprosil beads (inner diameter 75μm) with a gradient ramping from 2% to 54% ACN in 35 min, followed by a plateau at 72% ACN for 10 min and a subsequent plateau at 45% ACN for 5 min. MS data were acquired on a Q-Exactive HFX in data-dependent acquisition (DDA) with a top20 method. Full scan MS spectra were acquired at a resolution of 60,000 in the scan range from 350 to 1700 m/z, automated gain control (AGC) target was set to 3×10^6, and maximum injection time (IT) to 10 ms. MS/MS spectra were acquired at a resolution of 15,000, AGC target of 1×10^5, and maximum IT of 86 ms. Ions were isolated with a 1.3 m/z isolation window and normalized collision energy (NCE) was set to 26. Unassigned charge states and ions with a charge state of one, seven, or higher were excluded from fragmentation and dynamic exclusion was set to 20s.

PRISMA experiments

Cell lysates for PRISMA experiments

The goal of PRISMA experiments is to identify cytosolic proteins interacting with the intracellular tail of claudins. Therefore, we selected lysis conditions that enrich cytosolic content using a modified version of the Schreiber et al. (1989) nuclear-cytoplasmic fractionation protocol. First, confluent cultured MDCK-C7 cells were washed with cold PBS twice and incubated in trypsin for 1h. After cells were completely detached from the surface, they were harvested in a 15 mL tube and spun down at 600 xg, for 10 min at 4°C. Pelleted cells were then resuspended in 5 volumes of hypotonic Buffer A (5mM HEPES pH 8, 0.75mM $MgCl_2$, 5mM KCl, and cOmplete Mini protease inhibitor cocktail (Roche), supplemented with fresh 1mM DTT) and swollen on ice for 15 min. After the inubation, they are again spun down and resuspended in Buffer A supplemented with 1mM DTT and 0.5% DDM. Cells were passed through a 23G needle and incubated for 10 more min. Tubes were then centrifuged at 600 xg for 5 min at 4°C to precipitate the nuclei and the post-nuclear supernatant was transferred to a fresh tube. Two small aliquots were taken for estimation of the protein concentration and for Western blot analysis. The rest was snap-frozen and stored at −80°C until the PRISMA experiments were done.

PRISMA pull-downs

Protein interaction screen on a peptide matrix (PRISMA) was performed as described before (Dittmar et al., 2019) with slight adaptations of the protocol. Custom PepSpot cellulose membranes including peptides derived from the C-terminal tails of claudins were purchased from JPT (Berlin, Germany). According to the manufacturer, the synthetic peptides are prepared by SPOT-synthesis and each spot contains approximately 5 nmol peptide covalently bound to the cellulose-βalanine-membrane.

The experiment was done using three membranes, each of them containing 166 peptide spots (unmodified and phosphorylated) derived from the C-terminal cytosolic tail of claudins (Table S3). Membranes were pre-conditioned by incubation in membrane binding buffer (MBB) (5 mM HEPES pH 8, 0.75 mM $MgCl_2$, 5 mM KCl, and 1mM DTT), 45 min at RT in a plastic container in a rotator. Then, membranes were blocked with yeast tRNA (1 mg/mL in MBB), for 10 min at RT to minimize nonspecific binding to the cellulose membrane. To remove the tRNA excess, membranes were washed 5 times with MBB for 5 min at RT. Membranes were then incubated with the MDCK C7 cell extracts (3.5 mg/mL) for 20 min on ice, each membrane was incubated in a separate sealed bag. Prior to the incubation, a 20μg aliquot was taken from each cell extract tube to use as input samples. After incubation with the cell extracts, membranes were washed 3 times with MBB, 5 min at RT. Membranes were left to dry on a glass surface, then each spot was manually cut and transferred to a 96-well plate containing 20 μL of denaturation buffer (DB) (6M Urea, and 2M Thiourea in HEPES, pH 8). Spots containing the interacting proteins pulled down from the cell lysate were then subjected to in solution digestion.

In solution protein digestion

PRISMA samples were reduced and alkylated by incubation in 5mM final concentration of DTT (30 min at 37°C), followed by incubation in 15 mM final concentration IAA (45 min at RT, protected from light). Samples were then diluted in 50 mM ammonium bicarbonate (ABC) buffer to reduce the urea concentration down to 0.8 M and digested overnight with 0.5 μg trypsin at 37°C. After digestion, samples were acidified by adding 20 μL of 10%TFA to inactivate the trypsin. Samples were then stored at −20°C until the desalting and peptide clean-up step.

Peptide clean-up

After in solution digestion, PRISMA samples were desalted using Sep-Pak C18 96-well plates (Waters). Each step was followed by centrifugation of the 96-well plates for 1 min, at 1000 rpm, and at RT. First, the resin was pre-conditioned with 300 μL MeOH, followed by washing with 300 μL 80% ACN in water, and equilibrated twice with 300 μL 0.1% FA in water. Samples were then loaded and washed 5 times with 300 μL 0.1% FA in water. Desalted peptides were then eluted with 200 μL 50% ACN, 0.1% FA into 96-well plates (protein LoBind, Eppendorf), and dried with a vacuum centrifuge.

LC-MS/MS

Dried, desalted peptides were reconstituted in 30 μL of MS sample buffer (1% ACN/0.05% TFA.) and analyzed with a Dionex Ultimate 3000 RSLCnano coupled to a Q-Exactive HF mass spectrometer equipped with nano-electrospray ion source (Thermo Fisher Scientific). Samples were loaded onto a nanoEase M/Z Symmetry C18, 5 μm, 180 μm ID, 20 mm trap column (Waters) and separated onto a nanoEASE M/Z peptideBEH C18, 1.7 μm, 100 μm ID, 100 mm analytical column (Waters) with a gradient ramping from 10% to 40% ACN/FA 0.1% in 6min, followed by a plateau at 90% can/FA 0.1% for 2 min, total runtime 9.8 min. MS data was acquired by a Q-Exactive HF operated in DDA mode with a top10 method. Full scan MS spectra were acquired at a resolution of 60,000 at 200 m/z with a scan range of 375–1500 m/z, the AGC target was set to 3×10^6 charges and the maximum trapping time to 100 ms. MS/MS spectra were acquired at a resolution of 15,000 at 200 m/z, the AGC target was set to 1×10^5 charges, and maximum trapping time to 30 ms. Precursor ions were isolated with a 1.2 m/z isolation window by the quadrupole and normalized collision energy was set to 28. Unassigned charge states and ions with a charge state of 1, 6–8 or higher were excluded from fragmentation and dynamic exclusion was set to 7s.

Proximity ligation assays

Proximity ligation assays (PLA) were done using Duolink PLA reagents (DUO92007, DUO92002, and DUO92004 from Sigma-Aldrich) following the manufacturer's instructions. Briefly, three MDCK-C7 stable cell lines overexpressing claudin-1, claudin-3, and claudin-12 respectively were grown in glass slides until confluent. Similar to a standard immune-fluorescence sample preparation, cells were fixed with 4% PFA and permeabilized with 0.1% Triton X-100 in PBS. After this pre-treatment, cells were blocked with Duolink Blocking Solution for 1h at 37°C and subsequently incubated with the primary antibodies for detection of the YFP-claudin and the chaperonin containing TCP1 complex (CCT/TriC) or proteasome complex subunits respectively for 1h at RT (GFP, ab290, Abcam; TCP-1 β (CCT2), sc-374152; TCP1 Z (CCT6A), sc-514466; 20S proteasome α3 (PSMA3), sc-166205; Santa Cruz Biotechnology). Slides were washed 3 times for 1 min with Wash Buffer for Fluorescence A (Wash Buffer A) and incubated in PLA probe solution (PLUS and MINUS PLA Probes diluted 1:5 in Duolink Antibody diluent) for 1h at 37°C. Slides were washed again 3 times for 1 min with Wash Buffer A and incubated in ligation solution (Ligase 1:40 in 1x Ligation Buffer) for 30 min at 37°C. After three more washing steps with Wash Buffer A cells were incubated with amplification solution (Polymerase 1:80 in 1x Amplification Buffer) for 100 min at 37°C. Slides were finally washed with Wash Buffer for Fluorescence B (Wash Buffer B) protected from light, 3 times for 1min at RT, and one time with diluted 0.01x Wash Buffer B at RT. Slides were then mounted with 3-4μL of Duolink PLA Mounting Medium with DAPI, sealed with transparent nail polish, and stored until taken to the confocal microscope for imaging. In the case of PLA experiments on Caco2 cells, cells were fixed with 4% PFA after 24h of transfection. Cells were permeabilized, blocked, then incubated with a mix of anti-GFP (ab6556 from Abcam diluted at 1/1000 or 11,814,460,001 from Roche at 1/200) and anti-MCU (ab219827 from Abcam at 1/200) or anti-AFG3L2 (PA5-52080 from Invitrogen at 1/50) antibodies.

Slides were imaged on a Zeiss LSM 880 confocal microscope and images were acquired with a 63× oil immersion Plan-Apochromat objective 1.4 numerical aperture (Zeiss) and standard filter sets. Image analysis was performed with FIJI (ImageJ) according to published protocols (Gomes et al., 2016; Prado Martins et al., 2018). Briefly, single stack images were split into separate channels. The blue channel was used for nuclei counting while the red channel was for PLA signal retrieval. The average PLA signal per cell was obtained by dividing the total number of PLA dots by the number of nuclei in each image. 5 different fields were imaged per slide over 3 independent experiments.

QUANTIFICATION AND STATISTICAL ANALYSIS

MS data processing with MaxQuant

Raw files were analyzed using the MaxQuant version 1.5.2.8 searching against the *Canis lupus familiaris* UniProt database (2018). Settings were kept as default, methionine oxidation and deamidation (NQ) were included as a variable modification, cysteine carbamidomethylation as fixed modification, and quantitation was done using label-free quantification (Fast LFQ). 'match between runs' (MBR) was enabled to increase the number of identifications. The analysis of the CoIP raw data was done individually for each claudin isoform versus the GFP control using only unique peptides for quantification. For the PRISMA data, the search was done against an additional second database containing the C-terminal sequence of all human claudin isoforms to detect the synthetic tryptic peptides coming from the membrane. Input samples and groups of peptides from the same claudin were set to non-consecutive fractions so the MBR algorithm works only with runs within the same fraction.

Statistical analysis of MS data

After the MaxQuant analysis of the raw data the protein groups output files were filtered to remove potential contaminants, reverse hit, and proteins identified by site. In the case of the PRISMA dataset, C-terminal claudin peptides identified were also removed. The statistical analysis was done using the R software (R version 3.5.0, RStudio version 1.0.143) and the Proteomics Toolset for Integrative Data Analysis Shiny app (ProTIGY, Broad Institute).

CoIP data

Each claudin isoform dataset was filtered for proteins that were detected in at least 3 of the four replicates of each sample group (Claudin pull-down and eGFP control), and with at least two peptides. LFQ missing values were replaced using a downshift imputation approach (Keilhauer et al., 2015). LFQ intensity values of YFP-Claudin pull-downs were then compared against the GFP control by a two-sample moderated t test. First, we applied the standard significance cut-offs of 5% FDR and $\log_2$ fold change >1 for enrichment against the control. Based on the assumption that the eGFP protein has no specific interactors within the MDCK-C7 cells, a more stringent second level cut-off was applied at an adjusted p value that leaves only 5% of the interactions identified in the GFP control (Figure S2 and Table S1A).

PRISMA data

After the initial filtering of the dataset proteins identified only in the input samples were also removed. The following filtering for valid values and imputation of missing values was done as described for CoIP data and separately for the subset of PRISMA spots belonging to each claudin isoform. For the data analysis, moderated t test pairwise comparisons were done between the unmodified peptides from each claudin isoform on one hand, and between the unmodified and the phosphorylated versions of the same peptides on the other with a significance cut-off of 5% FDR. LFQ values of the significant interactors identified were normalized by *Z* score and plotted as a heatmap. This representation was used to manually select those proteins showing an intensity profile corresponding to the interaction with a SLiM, which means high LFQ values across 3 consecutive overlapping peptides with a maximum in the middle for the unmodified peptides (Figures 3F, S4, and S5; Tables 1B and S1C). For the study of PTMs, we selected those proteins that significantly showed a difference in the binding between the modified and the unmodified version of the same peptide (Figure 5B and Table S1D).

GO annotations and enrichment analysis

The list of significant interactors identified for each claudin was submitted to the online functional annotation tool DAVID (Huang et al., 2009a, 2009b). Using the gene names we looked for annotations of these interactors in human since the available data for *Canis lupus familiaris* contains many uncharacterized proteins. 708 out of 758 interactions were successfully annotated. Gene ontology (GO) terms related to cellular component (GOCC) were used to systematically classify the interactions identified by CoIP following an approach similar to the one used by (Tan et al., 2020). A hierarchical categorization was done looking first for annotations related to tight junction (GO:0005923, GO: 0061689) followed by adherens junction (GO: 0005913, GO:0005912), cell junction (GO:0005911, GO:0030054), apical plasma membrane (GO:0016324), basolateral plasma membrane (GO:0016323), cytoskeleton (GO:0005856, GO:0015629, GO:0015630, GO:0030863, GO:0045111), endosome/caveola/lysosome (GO:000576, GO:0005770, GO:0010008, GO:0005901, GO:0005764), integral component of plasma membrane, plasma membrane (GO:0005887), Golgi apparatus/vesicle/exosome (GO:0005794, GO:0000139, GO:0032588, GO:0005793, GO:0033116), ER(GO:0005783, GO:0005788, GO:0005789, GO:0030176), mitochondria (GO:0005739, GO:0005743, GO:0005741, GO:0005759), and nucleus (GO:0031965, GO:0005634, GO:0005654). Proteins that didn't contain any of these terms were categorized as "others" (Figure 2B and Table S1A).

Enrichment analysis of the significant interactions identified by CoIP was done using the Metascape gene annotation and analysis resource (Zhou et al., 2019). A multiple gene list was uploaded with the interacting partners identified for each claudin using *H. sapiens* as species. A custom analysis was done by selecting GO and KEGG terms in the Pathway and Structural complex sections for the enrichment analysis (Figure 2D).

Cell Reports, Volume *41*

Supplemental information

Pan-claudin family interactome analysis reveals shared and specific interactions

Lorena Suarez-Artiles, Tilman Breiderhoff, Rossana Girardello, Hannes Gonschior, Sophie Rodius, Antoine Lesur, Ulf Reimer, Evelyn Ramberger, Daniel Perez-Hernandez, Dominik Müller, Philipp Mertins, and Gunnar Dittmar

Supplemental information

Pan-claudin family interactome analysis reveals shared and specific interactions

Lorena Suarez-Artiles, Tilman Breiderhoff, Rossana Girardello, Hannes Gonschior, Sophie Rodius, Antoine Lesur, Ulf Reimer, Evelyn Ramberger, Daniel Perez-Hernandez, Dominik Müller, Philipp Mertins, and Gunnar Dittmar

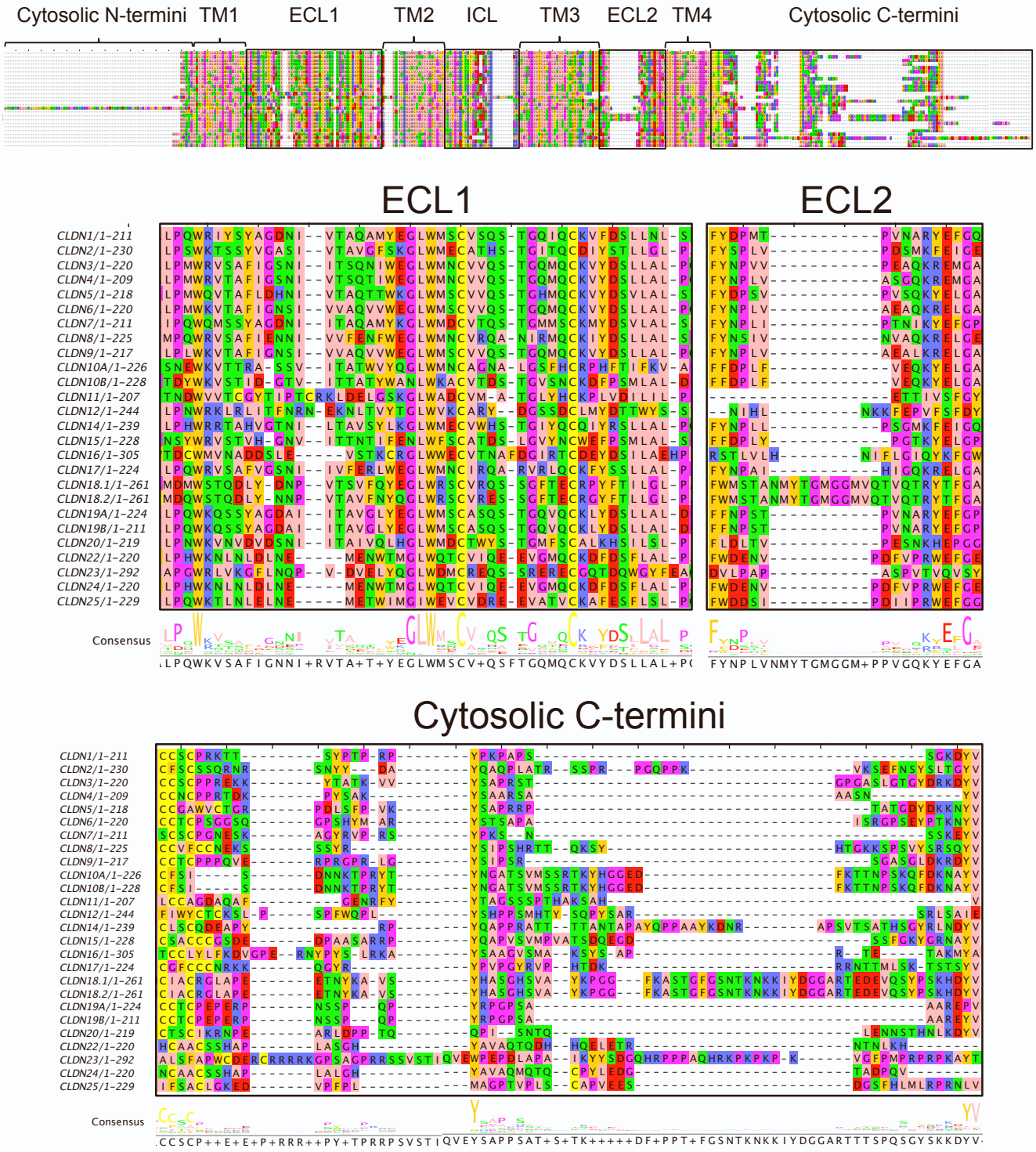

Figure S1 related to the introduction. Sequence alignment of all the claudins expressed in humans. The cytosolic C-termini tail of claudins show higher variability in length and sequence compared to more conserved regions like transmembrane domains (TM1-TM4) or extracellular loops (ECL1 and ECL2). TM: transmembrane. ECL: extracellular loop. ICL: intracellular loop.

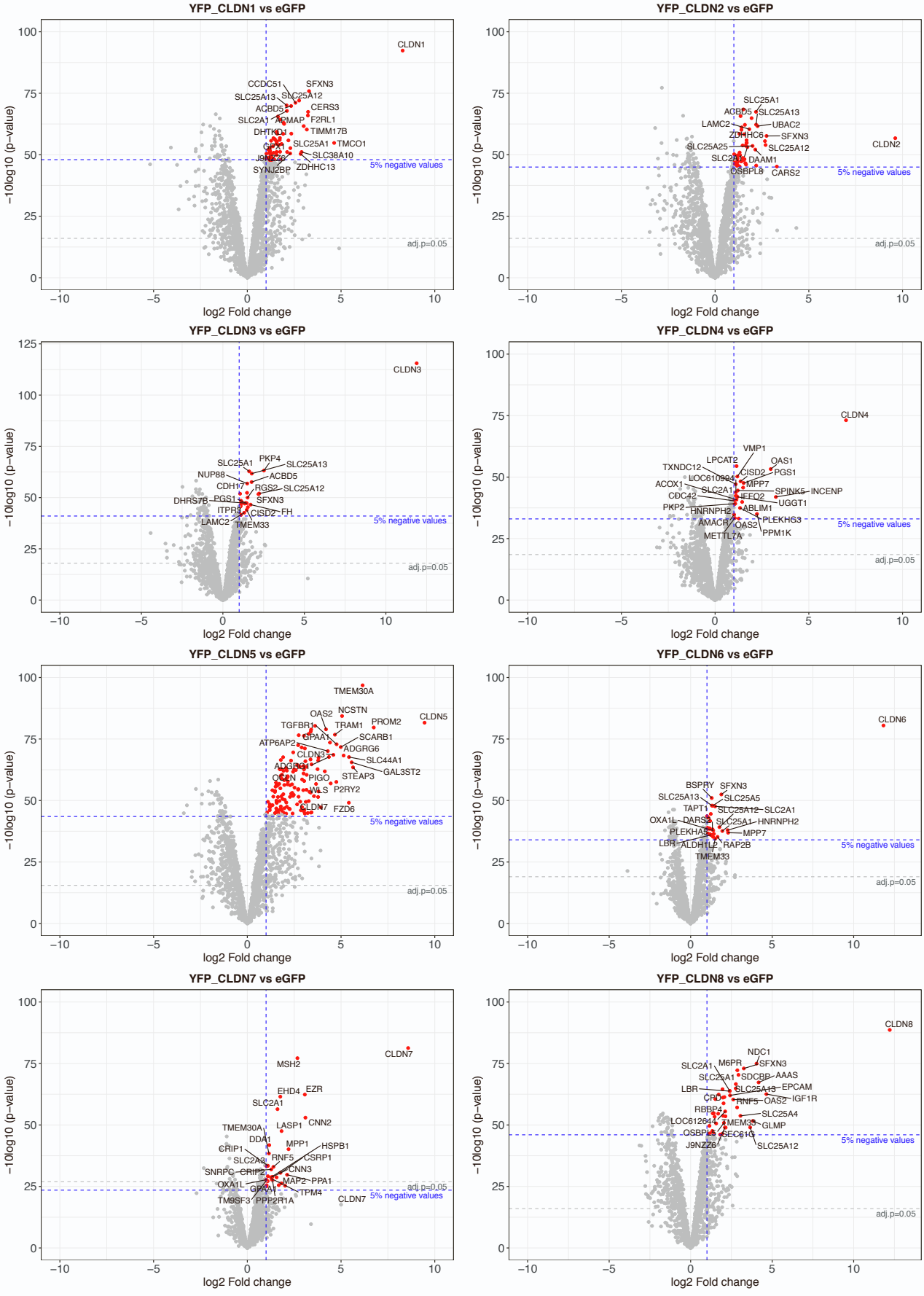
YFP_CLDN1 vs eGFP
YFP_CLDN2 vs eGFP
YFP_CLDN3 vs eGFP
YFP_CLDN4 vs eGFP
YFP_CLDN5 vs eGFP
YFP_CLDN6 vs eGFP
YFP_CLDN7 vs eGFP
YFP_CLDN8 vs eGFP
−10log10 (p−value)
log2 Fold change
5% negative values
adj.p=0.05
CLDN1
CLDN2
CLDN3
CLDN4
CLDN5
CLDN6
CLDN7
CLDN8

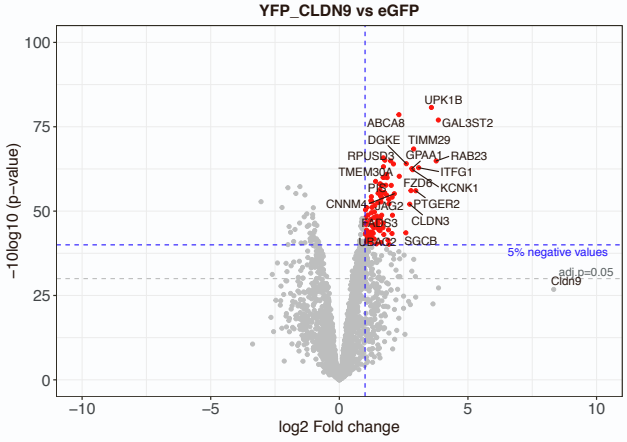
YFP_CLDN9 vs eGFP
−10log10 (p−value)
log2 Fold change
UPK1B
ABCA8
GAL3ST2
DGKE
TIMM29
RPUSD3
GPAA1
RAB23
TMEM30A
ITFG1
FZD6
KCNK1
CNNM4
PTGER2
FADS3
CLDN3
UBXN2
SGCB
5% negative values
adj.p=0.05
Cldn9

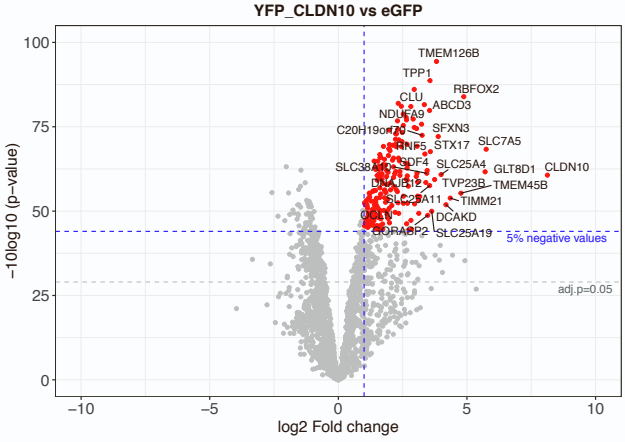
YFP_CLDN10 vs eGFP
−10log10 (p−value)
log2 Fold change
TMEM126B
TPP1
RBFOX2
CLU
ABCD3
NDUFA9
SFXN3
C20H19orf70
RNF5
STX17
SLC7A5
SLC38A10
SDF4
SLC25A4
GLT8D1
CLDN10
DNAJB12
TVP23B
TMEM45B
SLC25A11
TIMM21
OCIAD1
DCAKD
ARGRP2
SLC25A19
5% negative values
adj.p=0.05

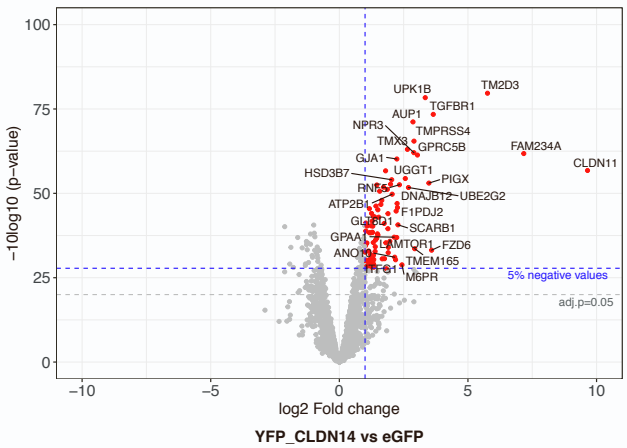
YFP_CLDN11 vs eGFP
−10log10 (p−value)
log2 Fold change
UPK1B
TM2D3
TGFBR1
AUP1
NPR3
TMPRSS4
TMX3
GPRC5B
FAM234A
GJA1
CLDN11
HSD3B7
UGGT1
PIGX
RNF5
DNAJB12
UBE2G2
ATP2B1
F1PDJ2
GLRX3
SCARB1
GPAA1
LAMTOR1
FZD6
ANO10
TMEM165
ITFG1
M6PR
5% negative values
adj.p=0.05

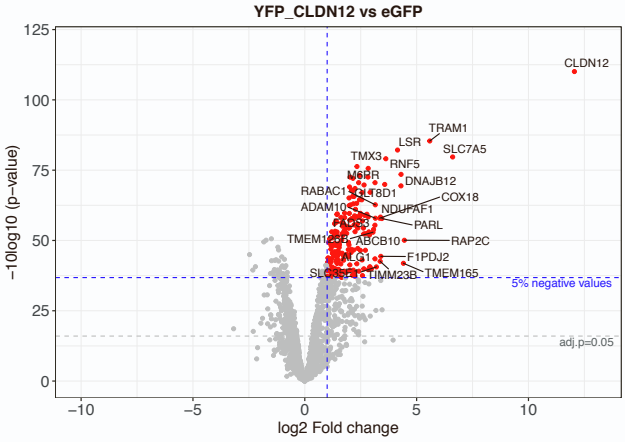
YFP_CLDN12 vs eGFP
−10log10 (p−value)
log2 Fold change
CLDN12
TRAM1
LSR
SLC7A5
TMX3
RNF5
USHR
DNAJB12
RABAC1
GLT8D1
COX18
ADAM10
NDUFAF1
PARL
TMEM126B
ABCB10
RAP2C
MLEC
F1PDJ2
SLC25A11
TIMM23B
TMEM165
5% negative values
adj.p=0.05

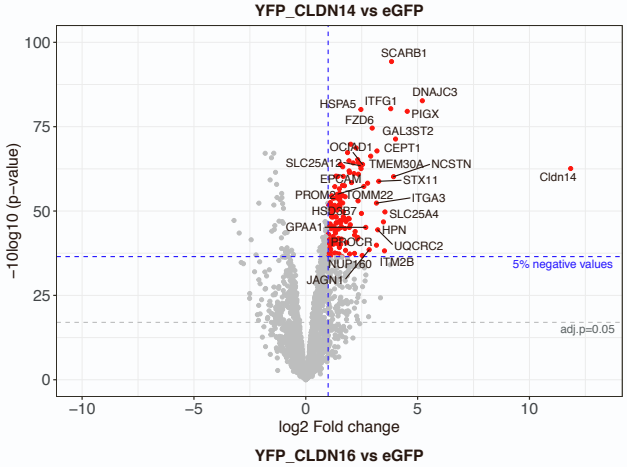
YFP_CLDN14 vs eGFP
−10log10 (p−value)
log2 Fold change
SCARB1
DNAJC3
HSPA5
ITFG1
PIGX
FZD6
GAL3ST2
OCIAD1
CEPT1
SLC25A12
TMEM30A
NCSTN
EPCAM
STX11
Cldn14
PROM2
TOMM22
ITGA3
HSD3B7
SLC25A4
GPAA1
HPN
PPOCR
UQCRC2
NUP160
ITM2B
JAGN1
5% negative values
adj.p=0.05

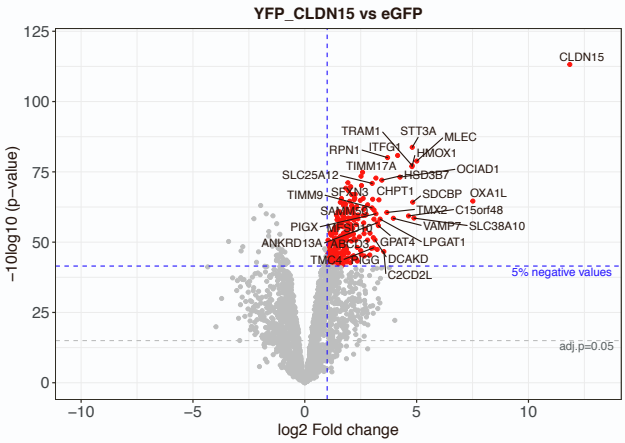
YFP_CLDN15 vs eGFP
−10log10 (p−value)
log2 Fold change
CLDN15
TRAM1
STT3A
MLEC
RPN1
ITFG1
HMOX1
TIMM17A
OCIAD1
SLC25A12
HSD3B7
TIMM9
CHPT1
SDCBP
OXA1L
SAMM50
TMX2
C15orf48
PIGX
VAMP7
SLC38A10
ANKRD13A
ABCD3
GPAT4
LPGAT1
TMCO1
ATG9
DCAKD
C2CD2L
5% negative values
adj.p=0.05

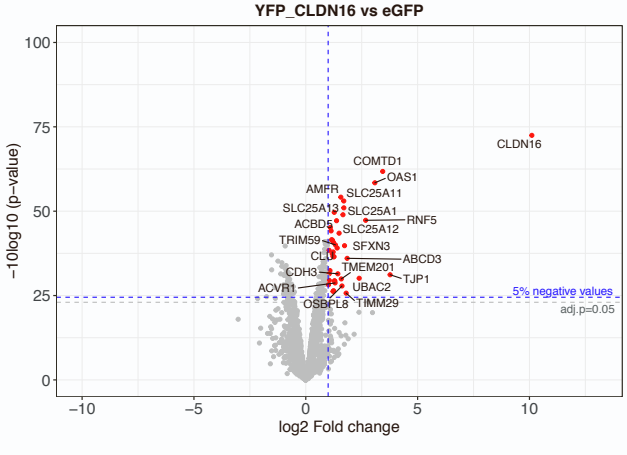
YFP_CLDN16 vs eGFP
−10log10 (p−value)
log2 Fold change
CLDN16
COMTD1
OAS1
AMFR
SLC25A11
SLC25A13
SLC25A1
RNF5
ACBD5
SLC25A12
TRIM59
SFXN3
CLU
ABCD3
TMEM201
CDH3
TJP1
AOVR1
UBAC2
OSBPL8
TIMM29
5% negative values
adj.p=0.05

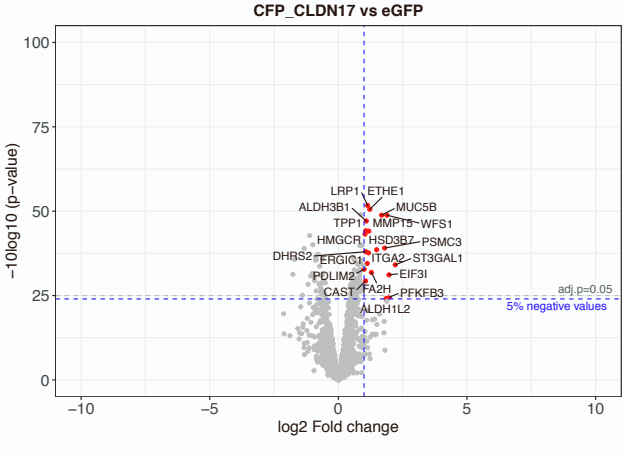
CFP_CLDN17 vs eGFP
−10log10 (p−value)
log2 Fold change
LRP1
ETHE1
ALDH3B1
MUC5B
TPP1
MMP15
WFS1
HMGCR
HSD3B7
PSMC3
DHRS2
ERGIC1
ITGA2
ST3GAL1
PDLIM2
EIF3I
CAST
FA2H
PFKFB3
ALDH1L2
adj.p=0.05
5% negative values

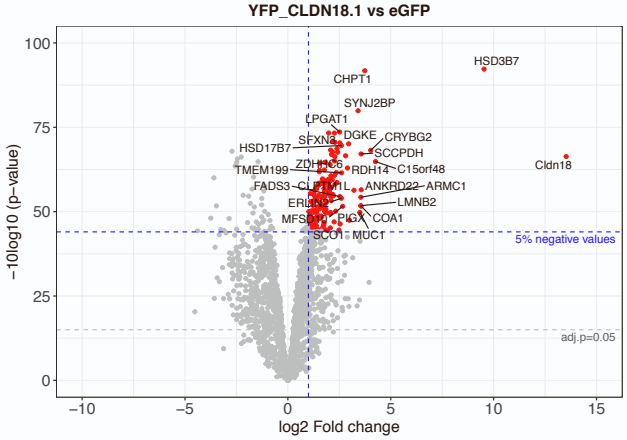
YFP_CLDN18.1 vs eGFP
HSD3B7
CHPT1
SYNJ2BP
LPGAT1
DGKE
CRYBG2
SFXN3
SCCPDH
HSD17B7
ZDHHC6
RDH14
C15orf48
TMEM199
Cldn18
FADS3
CLPTM1L
ANKRD22
ARMC1
ERLIN2
LMNB2
MFSD11
PIGX
COA1
SCO1
MUC1
5% negative values
adj.p=0.05
−10log10 (p−value)
log2 Fold change

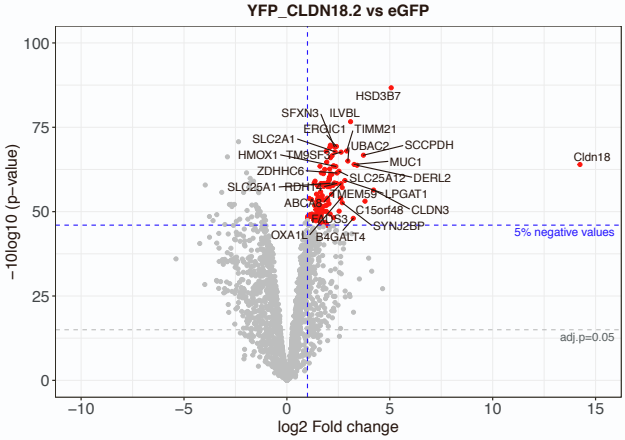
YFP_CLDN18.2 vs eGFP
HSD3B7
SFXN3
ILVBL
ERGIC1
TIMM21
SLC2A1
UBAC2
SCCPDH
HMOX1
TM9SF3
MUC1
Cldn18
ZDHHC6
SLC25A12
DERL2
SLC25A1
RDH14
TMEM59
LPGAT1
ABCA5
C15orf48
CLDN3
FADS3
SYNJ2BP
OXA1L
B4GALT4
5% negative values
adj.p=0.05
−10log10 (p−value)
log2 Fold change

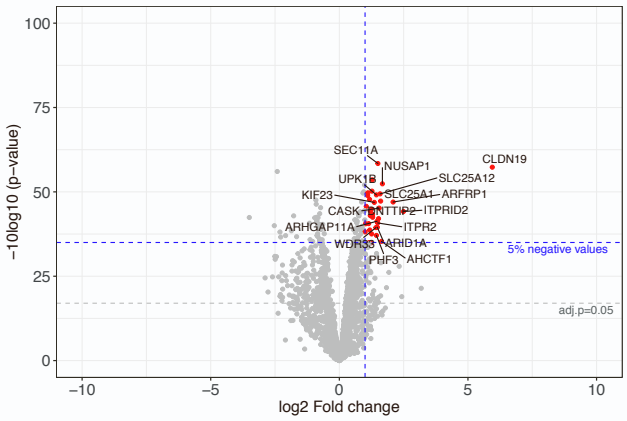
CFP_CLDN19a vs eGFP
SEC11A
NUSAP1
CLDN19
UPK1B
SLC25A12
KIF23
SLC25A1
ARFRP1
CASK
ITPRID2
ARHGAP11A
ITPR2
WDR33
ARID1A
PHF3
AHCTF1
5% negative values
adj.p=0.05
−10log10 (p−value)
log2 Fold change

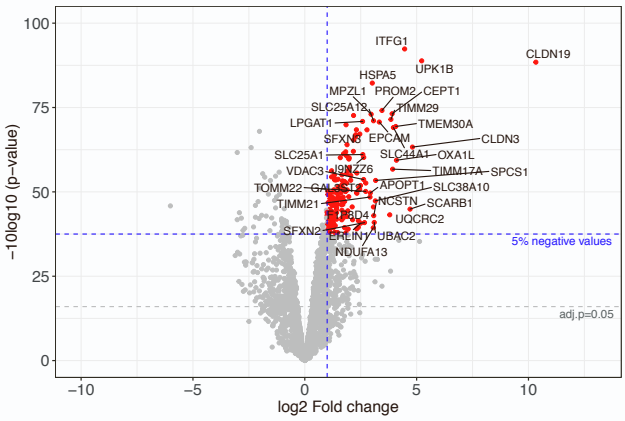
YFP_CLDN19b vs eGFP
ITFG1
CLDN19
UPK1B
HSPA5
MPZL1
PROM2
CEPT1
SLC25A13
TIMM29
LPGAT1
TMEM30A
SFXN3
EPCAM
CLDN3
SLC25A1
SLC44A1
OXA1L
VDAC3
TIMM17A
SPCS1
TOMM22
APOPT1
SLC38A10
TIMM21
NCSTN
SCARB1
UQCRC2
SFXN2
ERLIN1
UBAC2
NDUFA13
5% negative values
adj.p=0.05
−10log10 (p−value)
log2 Fold change

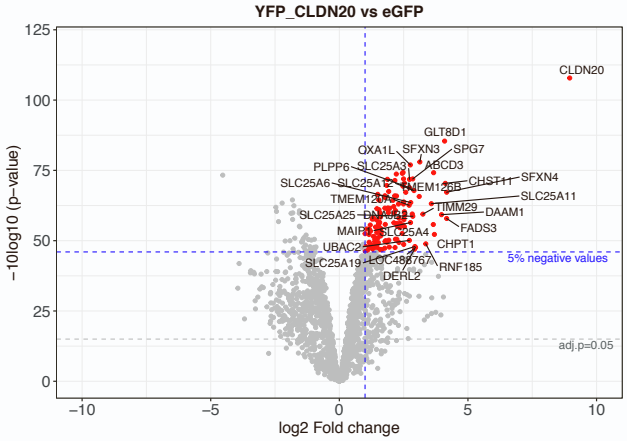
YFP_CLDN20 vs eGFP
CLDN20
GLT8D1
OXA1L
SFXN3
SPG7
PLPP6
SLC25A3
ABCD3
SLC25A6
SLC25A4
CHST11
SFXN4
TMEM126B
TMEM126A
SLC25A11
SLC25A25
TIMM29
DAAM1
MAIP1
FADS3
UBAC2
CHPT1
SLC25A19
LOC485767
RNF185
DERL2
5% negative values
adj.p=0.05
−10log10 (p−value)
log2 Fold change

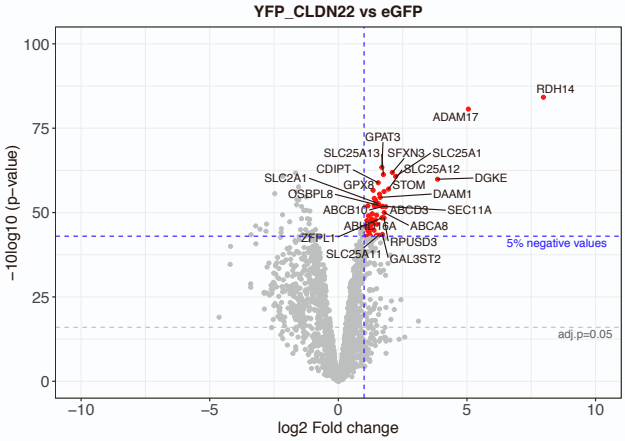
YFP_CLDN22 vs eGFP
RDH14
ADAM17
GPAT3
SLC25A13
SFXN3
SLC25A1
CDIPT
SLC25A12
SLC2A1
GPX8
STOM
DGKE
OSBPL8
DAAM1
ABCB10
ABCD3
SEC11A
ABHD16A
ABCA8
ZFPL1
RPUSD3
SLC25A11
GAL3ST2
5% negative values
adj.p=0.05
−10log10 (p−value)
log2 Fold change

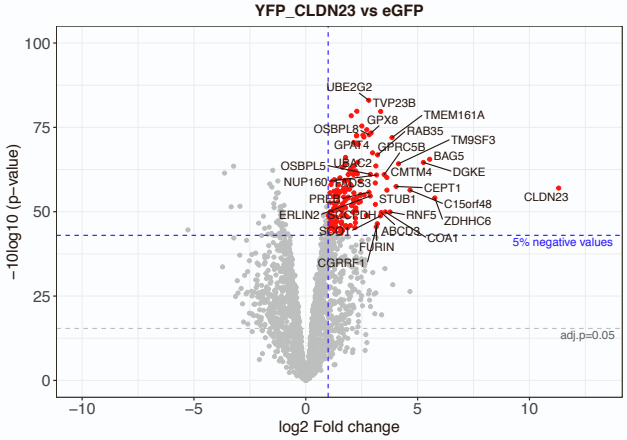
YFP_CLDN23 vs eGFP
UBE2G2
TVP23B
GPX8
TMEM161A
OSBPL8
RAB35
TM9SF3
GPAT4
GPRC5B
BAG5
OSBPL5
UBAC2
CMTM4
DGKE
NUP160
FADS3
CEPT1
PREB
STUB1
C15orf48
CLDN23
ERLIN2
SCCPDH
RNF5
ZDHHC6
SCO1
ABCD3
COA1
FURIN
CGRRF1
5% negative values
adj.p=0.05
−10log10 (p−value)
log2 Fold change

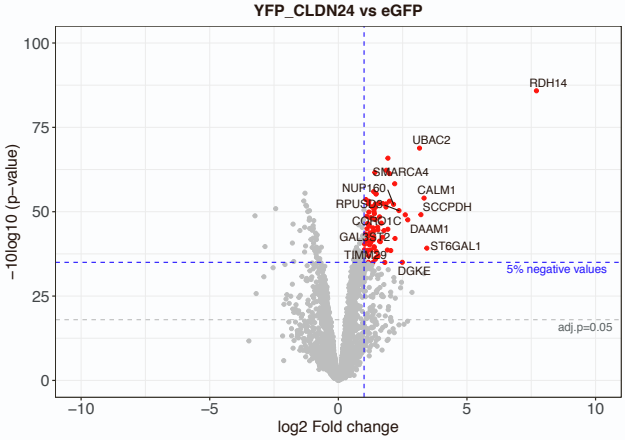
YFP_CLDN24 vs eGFP
RDH14
UBAC2
SMARCA4
NUP160
CALM1
RPUSD4
SCCPDH
CGRRF1
DAAM1
GAL3ST2
ST6GALNAC2
TIMM29
DGKE
5% negative values
adj.p=0.05
−10log10 (p−value)
log2 Fold change

Figure S2, related to Figure 2. Volcano plots showing the results from all CoIP experiments. LFQ intensity values of YFP/CFP-Claudin pull-downs were compared against the GFP control using moderated t-test. First significance level adj-pval<0.05 (grey line), 2nd level cutoff of adj-pval that leaves only 5% of the interactions identified in the GFP control (blue line).

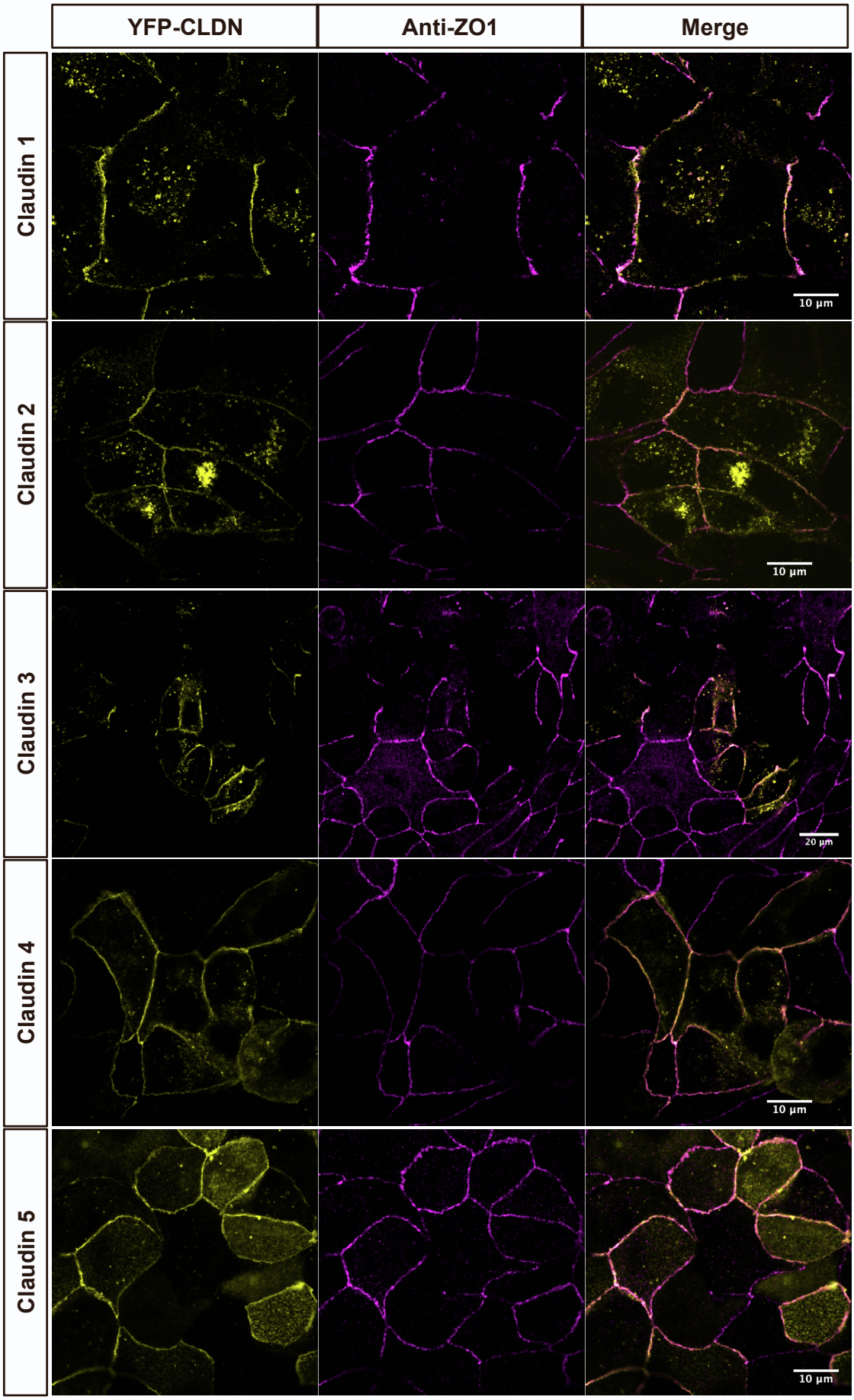
YFP-CLDN
Anti-ZO1
Merge
Claudin 1
Claudin 2
Claudin 3
Claudin 4
Claudin 5
10 µm
10 µm
20 µm
10 µm
10 µm

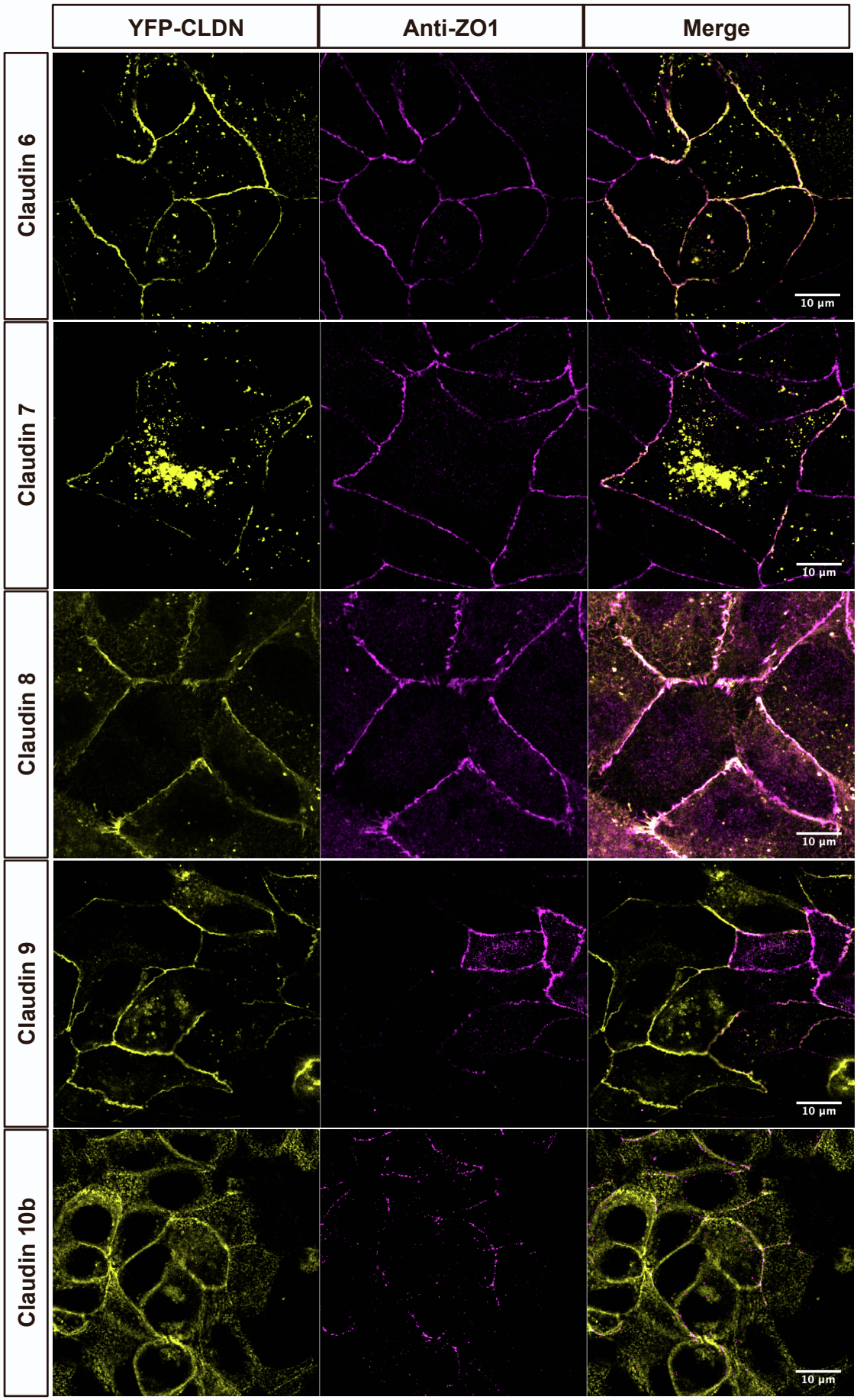
YFP-CLDN
Anti-ZO1
Merge
Claudin 6
Claudin 7
Claudin 8
Claudin 9
Claudin 10b
10 µm
10 µm
10 µm
10 µm
10 µm

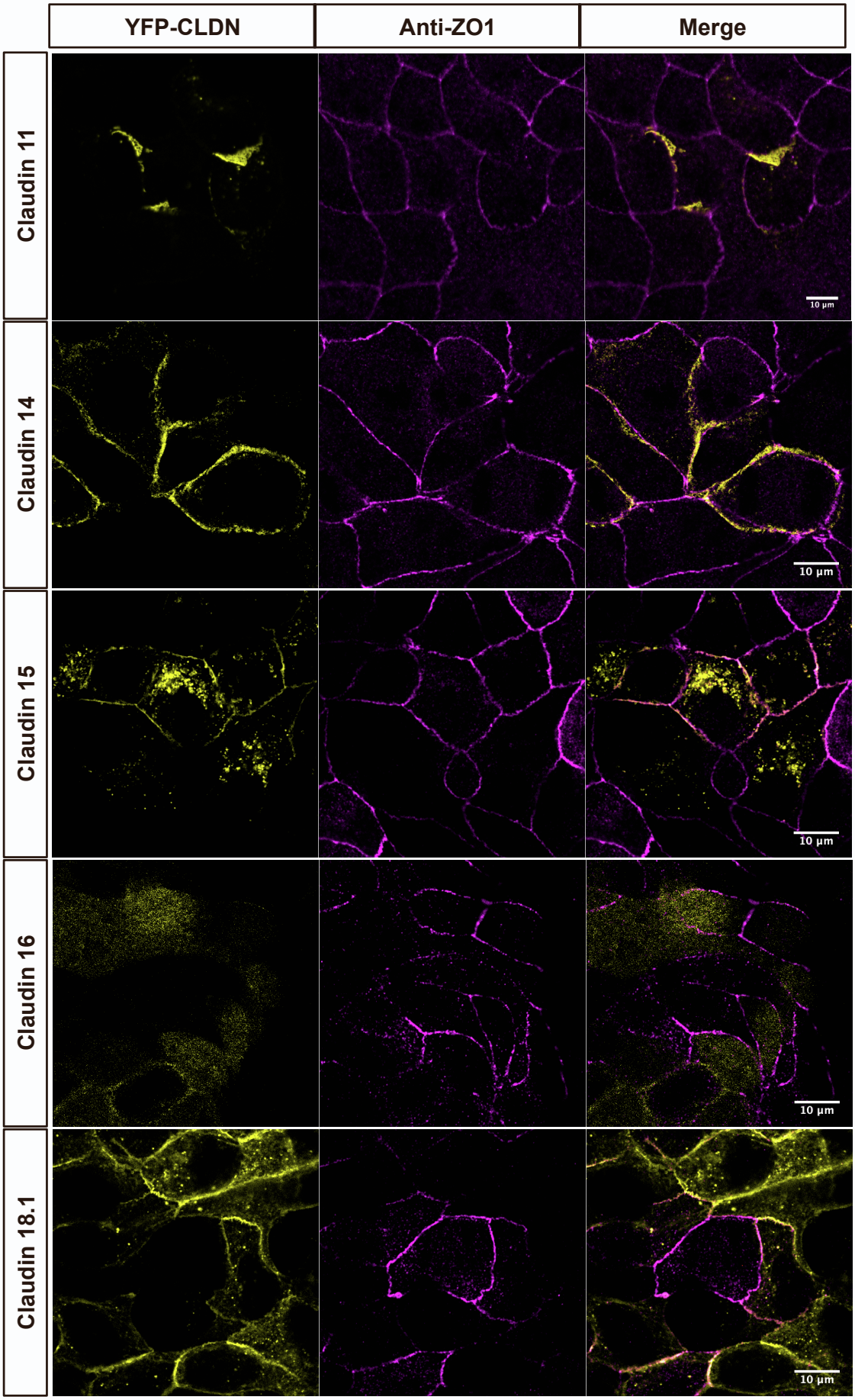
YFP-CLDN
Anti-ZO1
Merge
Claudin 11
Claudin 14
Claudin 15
Claudin 16
Claudin 18.1
10 µm

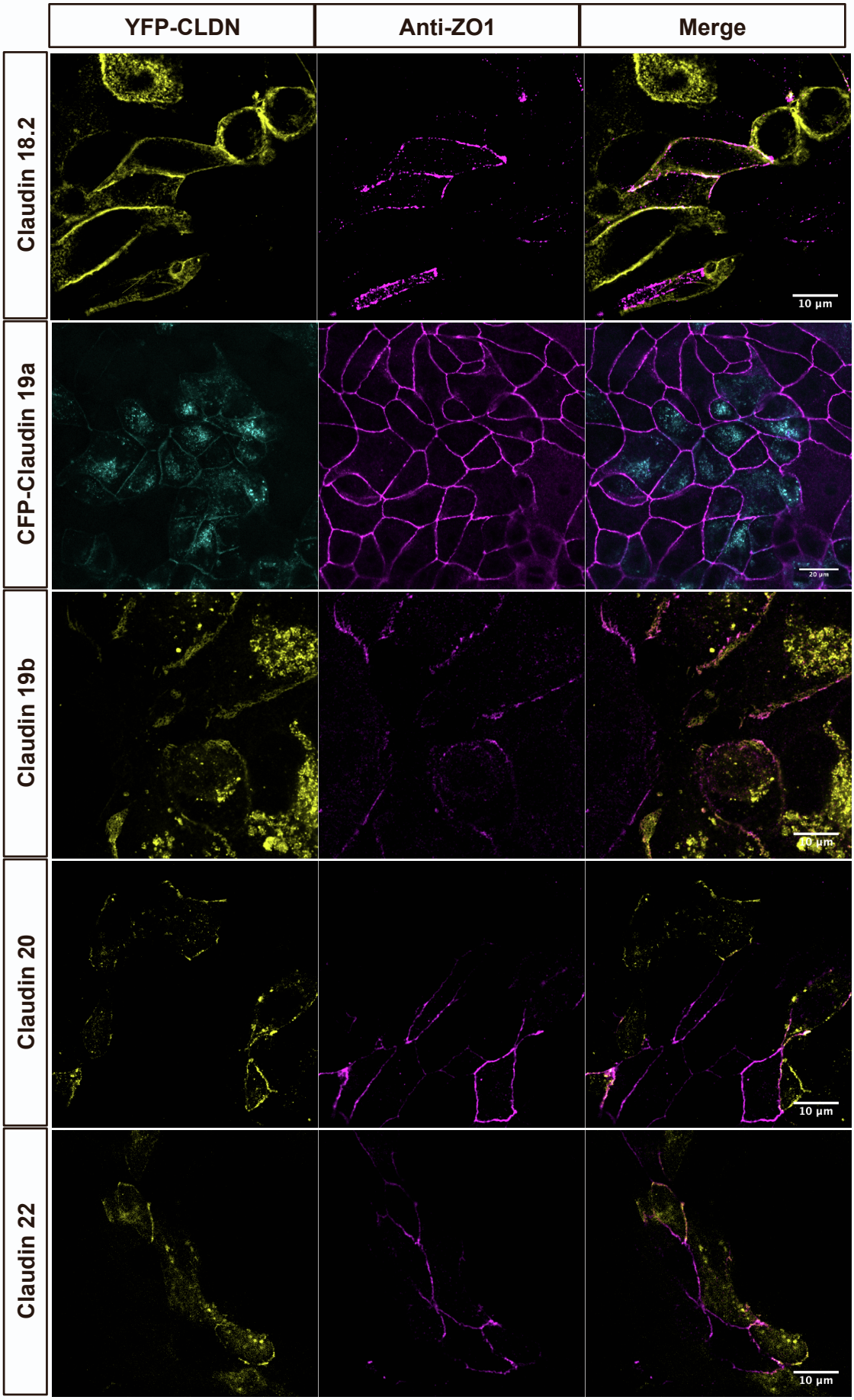
YFP-CLDN
Anti-ZO1
Merge
Claudin 18.2
CFP-Claudin 19a
Claudin 19b
Claudin 20
Claudin 22
10 µm
20 µm
10 µm
10 µm
10 µm

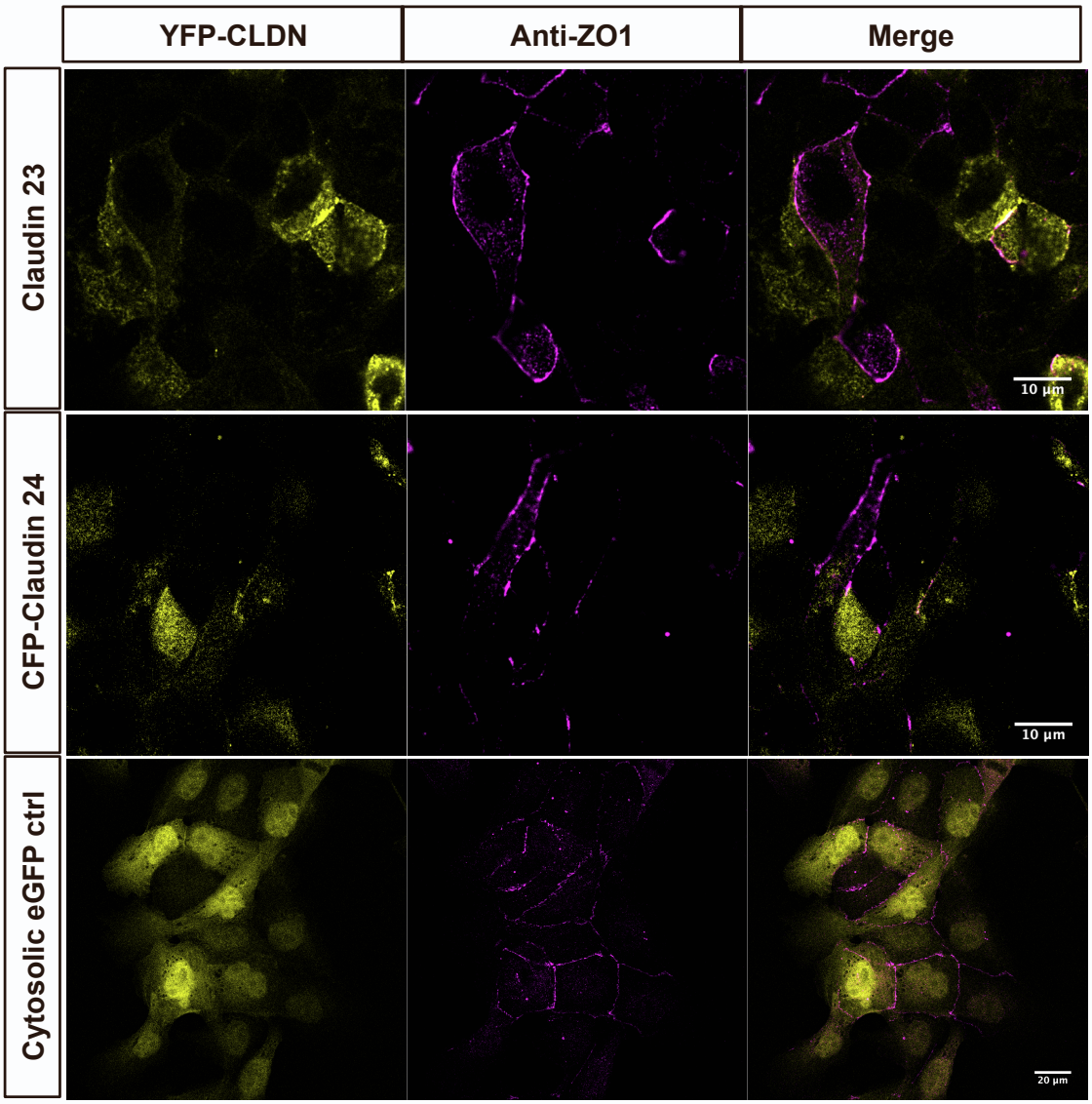

Figure S3, related to Figure 2. Confocal microscopy images of MDCK-C7 stable cell lines overexpressing recombinant YFP-/CFP- claudins. Anti-ZO-1 (61-7300 Invitrogen) and Alexa Fluor® 647 were used for tight junction staining.

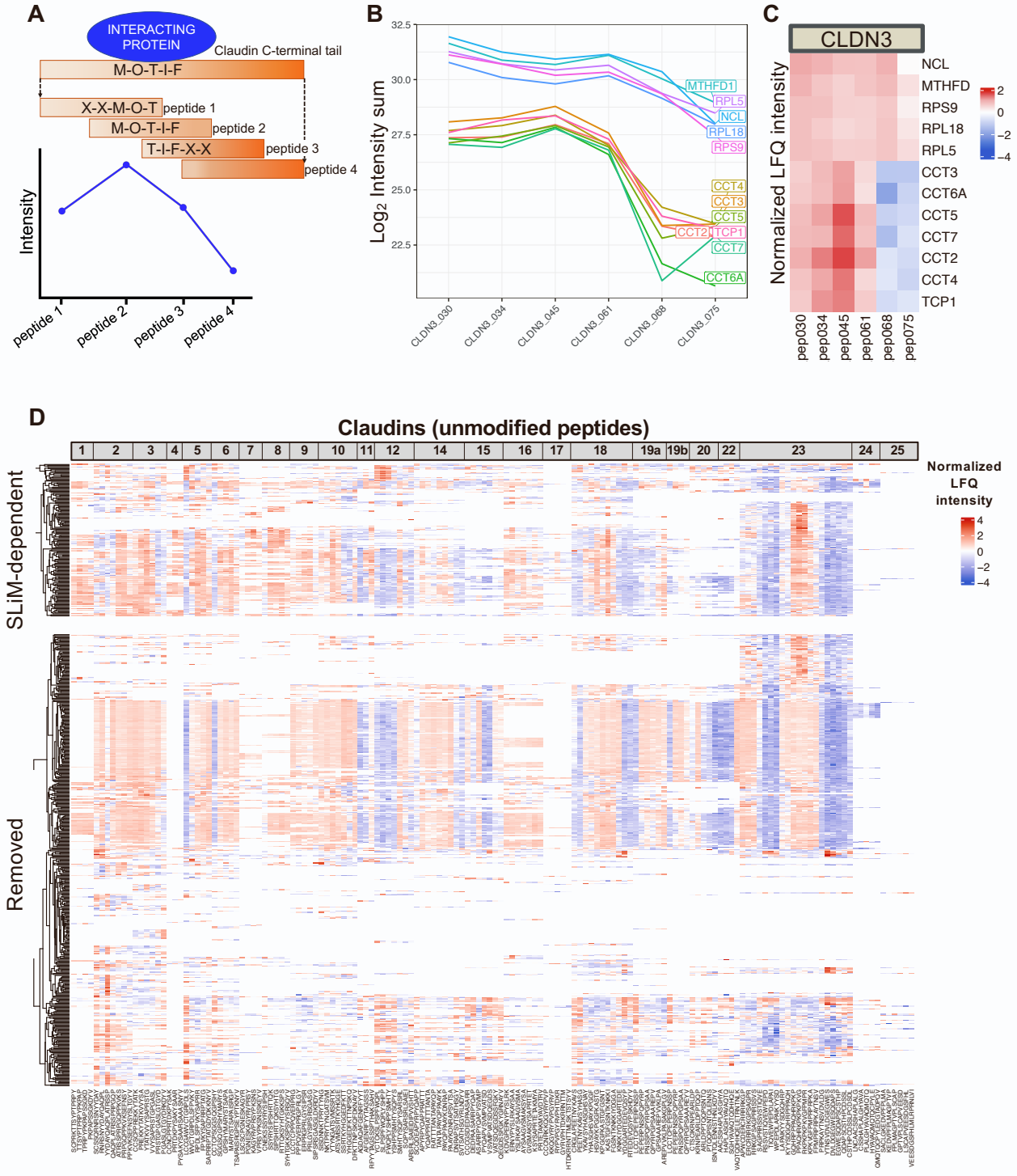

Figure S4, related to Figure 3. Filtering strategy for SLiM-dependent interactors identified by PRISMA. **A.** Schematic representation of the SLiM-based intensity profile pattern used to filter significant PRISMA interactions. **B, C.** Example of the intensity profile of filtered (highly abundant unspecific proteins) and SLiM-dependent (CCT/TriC subunits) significant claudin interactors. **D.** Heatmap showing all the significant interactors identified by PRISMA with the SLiM-dependent interactors on top (based on their intensity profile) and the interactions that were removed after the filtering process.

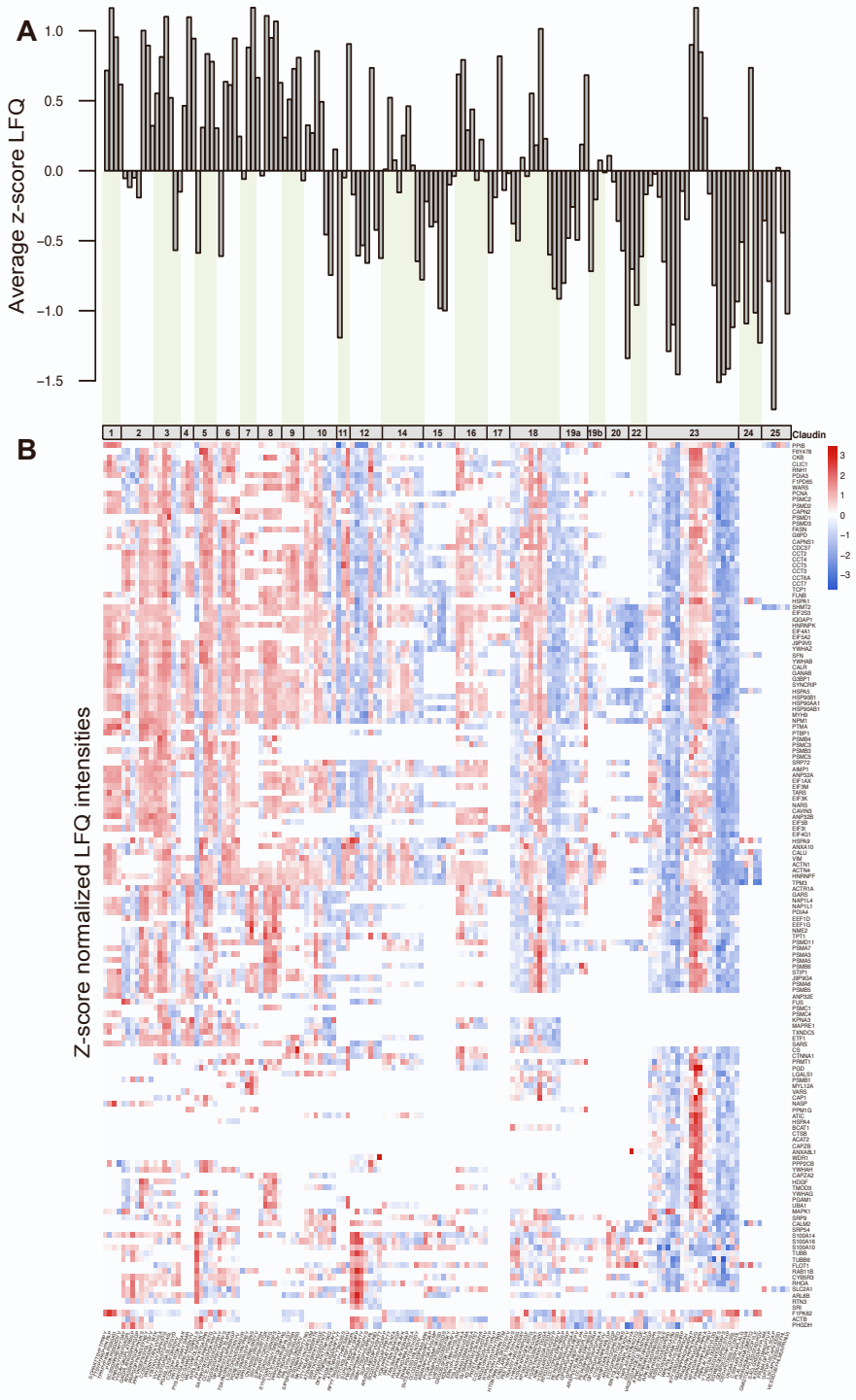

Figure S5, related to Figure 3. Interacting partners of the unstructured C-termini of claudins identified by PRISMA. A. Bar plot corresponding to the normalized intensities of the significant interactions (p-value<0.05 and intensity binding profile) identified per peptide spot. **B.** Heatmap showing the interaction patterns of the significant proteins identified interacting with unmodified peptides derived from the C-terminal region of human claudins.

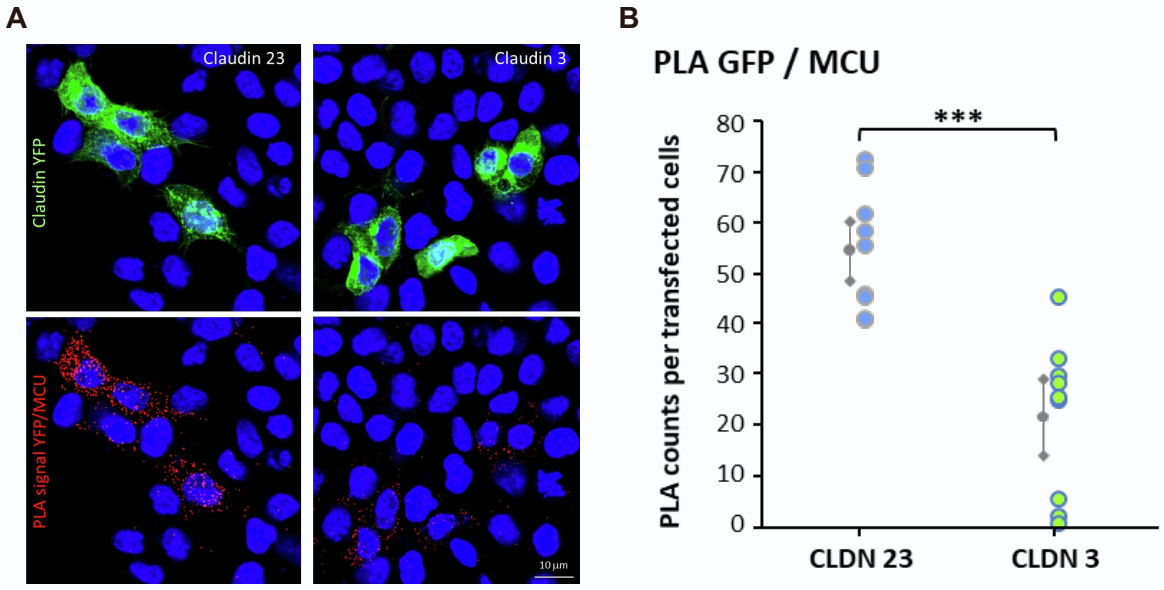

Figure S6, related to Figure 4. Proximity ligation assay confirms interaction between claudin-23 and the mitochondrial protein MCU. A. Immunofluorescence images of PLA between MCU and claudin-23 or claudin-3. Caco2 cells were transiently transfected with YFP-tagged claudin-23 or claudin-3. MCU mitochondrial protein interacts with claudin-23 but not with claudin-3. **B.** Dot plot representing the number of PLA signals per transfected cell. Statistically significant results ($P<0.05$) confirm those of the YFP-tagged claudin-23 CoIP .